

ELECTROWETTING ON DIELECTRIC (EWOD)
DIGITAL MICROFLUIDICS FOR
ELECTRONIC HOTSPOT
COOLING

by

GOVINDRAJ SHREYAS BINDIGANAVALA

Presented to the faculty of the Graduate School of
The University of Texas at Arlington in Partial Fulfillment
of the Requirements
for the Degree of

MASTER OF SCIENCE IN MECHANICAL ENGINEERING

THE UNIVERSITY OF TEXAS AT ARLINGTON

December 2009

Copyright © by Govindraj Shreyas Bindiganavale 2009

All Rights Reserved

ACKNOWLEDGEMENTS

Firstly, I would like to thank Dr. Moon for guiding and advising me throughout my research and giving me the opportunity to learn skills from varied fields of Engineering. I specially thank Dr. Liu from the Mechanical and Aerospace Engineering, UTA and Dr. Armstrong from the Department of Chemistry and Physics, UTA for assisting me in my research work and Dr. You for being part of my defense committee. I thank my team mates, Manohara Mariyappa, Yasith Nanayakarra and Jagath Nikapitiya, for providing data crucial to my research. I am also grateful to Hans Landsberger for reviewing and helping me write my thesis.

Working at the Integrated Micro & Nanofluidic Systems Lab wouldn't have been fun if it weren't for my lab mates. I would like to thank Nitin Garg, Praveen Kunchala, Subin George, Hans and Jagath in this regard.

Last but not the least; I extend my acknowledgements to all my friends and family members for their help and support. Finally, I am indebted to my parents for all the love and blessings they gave me throughout my life.

November 20, 2009

ABSTRACT

ELECTROWETTING ON DIELECTRIC (EWOD)
DIGITAL MICROFLUIDICS FOR
ELECTRONIC HOTSPOT
COOLING

Govindraj Shreyas Bindiganavale, M.S.

The University of Texas at Arlington, 2009

Supervising Professor: Hyejin Moon

Electronics cooling was a field dominated by bulky and heavy heat sinks, heat pipes and fans for decades. Lately, the size of the electronic components has decreased to a substantial extent with an increase in performance. This has fuelled a need for smaller, lighter, yet efficient cooling systems. A lot of research has been done to build innovative cooling solutions which satisfied most of the requirements as stated above. Some of them still have limitations like use of the right coolants and design challenges. Digital microfluidics is one field which can solve all these issues by providing a simple, reliable and efficient way of pumping coolants over hotspots. For this purpose, a microfluidic hotspot cooling device was fabricated which used special liquids called Ionic Liquids (IL's) as coolants. Unlike other coolants used, IL's has the property of being thermally stable at elevated temperatures and chemically inert to most of the known metals.

This thesis report describes the performance of IL's in the device for hotspot cooling. Liquid Crystal Thermographical analysis was performed in order to estimate the temperatures of the hotspot and heat removal and heat conduction rate calculations were performed based on

the analysis. In order to check the quality of the results, a comparison was made with the results of DI water.

It was observed that DI water emerged as the best liquid for hotspot cooling and IL's performed poorly. This was due to the high heat capacities and thermal conductivities of water. In order to get better results for IL's, it was concluded that the thermal conductivity values should emulate that of water's values. Adding CNT's (Carbon Nanotubes) to the IL can help us in this regard. Moreover, as the heat removal rate was a rough calculation, it was hard to estimate an accurate rate for the DI water and IL. Efforts are being made to come up with a realistic approach towards estimation of this data.

In future, by increasing the thermal conductivities of IL's and using advanced methods to perform the analysis with an improvement in design of the hotspot cooling device, cooling hotspots in small, compact and powerful electronic devices can become a reality.

TABLE OF CONTENTS

ACKNOWLEDGEMENTS	iii
ABSTRACT	iv
LIST OF FIGURES	viii
LIST OF TABLES	xi
Chapter	Page
1. INTRODUCTION	1
1.1 Electronics Cooling	1
1.2 Electrowetting and Electrowetting on Dielectric (EWOD)	1
1.2.1 Microfluidic Hotspot Cooling Device using EWOD Principle	3
1.3 Ionic Liquids (IL's)	4
1.3.1 Ionic Liquids for Electronic Hotspot Cooling	4
1.3.2 Electrowetting Experiments on IL's	5
1.3.3 AC EWOD curves for IL's	7
2. DIGITAL MICROFLUIDIC DEVICE	10
2.1 Device Setup	10
2.2 Heater and EWOD Circuit Designs	13
2.3 Device Fabrication	15
3. EXPERIMENTAL	19
3.1 Hardware and Software	19
3.2 Experimental Procedure	22
3.3 Data Collection and Organization	26
4. ANALYSIS AND RESULTS	27

4.1 Qualitative Analysis – Liquid Crystal Thermography (LCT)	27
4.1.1 RGB to HSI/HSL/HSV Color Space Conversion using LabVIEW and NI Vision Assistant	30
4.1.2 LCT using Image Processing Toolbox in MATLAB	35
4.1.3 Temperature – Color Representation and Calibration	39
4.1.4 LCT Results	41
4.2 Quantitative Analysis	47
4.2.1 Heat Removing Capacity	48
4.2.2 Heat Transferred through Conduction	50
4.2.3 Results	55
4.3 Conclusions and Future Work	55
APPENDIX	
A. MATLAB CODE FOR LCT	57
REFERENCES	60
BIOGRAPHICAL INFORMATION	62

LIST OF FIGURES

Figure	Page
1.1 EWOD effect on a hydrophobic surface showing the drop before (a) and after (b) applying electric field	2
1.2 Concept of hotspot cooling by EWOD ((a) through (d)) showing heat removal by the cool drop	4
1.3 Experimental setup of contact angle measurements of IL's using goniometer	6
1.4 An ideal EWOD curve showing the actual trend in blue and desired in red	7
1.5 EWOD curves of all the liquids tested. IL3 and IL4 have the best results	8
2.1 Cross section view of microfluidic device for hotspot cooling with the corresponding thickness	10
2.2 Figure showing the isometric view of the hotspot cooling device	11
2.3 Top chip PCB showing the etched copper electrodes	12
2.4 Mask showing two EWOD sets and one heater set used in photo lithography for cooling device fabrication	13
2.5 Set 1 (a) and set 2 (b) EWOD designs with heater (c) set	14
2.6 Figure showing the fabrication process	16
2.7 ITO patterned bottom and top chips compared to a 5 cent coin	17
2.8 Cross section of the top and bottom chips after fabrication	18
3.1 Flowchart showing the hardware and software components of the entire setup. Dark arrows represent digital and electrical signals while dotted arrows represent visual data	19
3.2 Custom built switch board showing the connector sockets and switches	20
3.3 Overview of the hardware and software setup	21
3.4 An RTIL1 drop sandwiched between the top and bottom chip, ready for the experiment. The ground electrode is slightly visible as its out of focus	23

3.5	DAQ Assistant interface in LabVIEW showing nine ports assigned to the digital I/O device	24
3.6	Custom built VI showing the block diagram for image acquisition and processing	25
4.1	Figure showing TLC painted behind the glass creating a color contour when hotspot was switched on	28
4.2	Figure showing the three stages in which LCT analysis was performed	29
4.3	Figure showing the HSL and HSV color wheel. Hue is independent of lighting	31
4.4	Separated color planes of an HSV image with the original RGB image and the angle of the color on the hue color wheel	32
4.5	Error in RGB (a) to hue (b) conversion due to presence of pink color in the outermost red band in (a)	33
4.6	Phase shift of RGB line to a safe negative value	33
4.7	RGB image after the RGB shift (a) and the correct hue image with the red band showing the lowest intensity (b)	34
4.8	Custom built LabVIEW VI showing the different VI's used for RGB to HSL conversion and Vision Assistant VI for filtering	34
4.9	A hue image with noise surrounding the hotspot (a) and the filtered image with a considerable reduction in noise (b)	35
4.10	RGB image showing the resolution on X and Y axis	36
4.11	Figure showing the variable editor (left) with the pixel intensity values of RGB variable with the workspace window (right) showing the dimensions of the variables	36
4.12	Hue image of the sample 100x30 RGB image with gray scale color bar with 256 shades	37
4.13	The contour plot of the hue image with the color bar purely based on the intensity values of H2	38
4.14	Temperature obtained at various color bands on the hot spot by using a thermocouple	39
4.15	Hue image (a) and the corresponding temperature contour (b)	40
4.16	A DI water drop without (a) and with (b) silicone oil shell surrounded by satellite drops due to phase change effects	42

4.17	Shifted RGB and actual LCT images of pure DI water just before moving on the hotspot [(a), (b)] and after moving onto the hotspot [(c), (d)]	43
4.18	Shifted RGB and actual LCT images of pure DI water with oil shell just before cooling [(a), (b)] and after moving onto the hotspot [(c), (d)]	44
4.19	Shifted RGB and actual LCT images of IL1 just before cooling [(a), (b)] and after moving onto the hotspot [(c), (d)]	45
4.20	Shifted RGB and actual LCT images of pure IL2 just before cooling [(a), (b)] and after moving onto the hotspot [(c), (d)]	46
4.21	Shifted RGB and actual LCT images of IL3 just before cooling [(a), (b)] and after moving onto the hotspot [(c), (d)]	47
4.22	Modeling the drop as a cylinder for convenience	48
4.23	Figure showing the pixels estimation in each color band on the LCT image	50
4.24	Actual dimensions of the LCT image displayed at normal zoom	51
4.25	Figure showing the temperature and area of each color band on the hotspot (2-D) and the temperature distribution in the drop (3-D). The x in T_{1x} takes variables from a to h	52
4.26	Estimation of A_c by subtracting A_d , A_e , A_f , A_g and A_h	53

LIST OF TABLES

Table		Page
1.1	Structures of Ionic Liquids used with some properties	5
4.1	Pixel intensity combinations giving rise to various colors	30
4.2	Table showing the heat removal rate for all the drops tested in the hotspot cooling device	49
4.3	Table showing the net heat transferred through conduction	54

CHAPTER 1

INTRODUCTION

1.1 Electronics Cooling

Over the years, we have seen a tremendous improvement in the size reduction of electronic devices and components. In addition to size reduction, there has also been a marked increase in both the number of operations that can be performed as well as increased heat generation. One of the primary factors deciding the reliability of any electronic device today is the amount of heat it can expel per unit watt of power generated. This relies solely on the means of cooling systems utilized to dissipate the device. Conventional cooling systems include heat sinks¹, heat pipes², fans and vent assemblies, which are found in majority of the electronic devices today. Due to the fact that these components are bulky and heavy, researchers are developing small, lightweight and more efficient cooling solutions compatible with the ever diminishing size of electronics, yet keeping them within thermal specifications.

Researchers in the field of electronics cooling have developed and demonstrated cooling systems which are smaller, lighter and more efficient than the traditional heat pipe/heat sink mechanism. Such technologies include, but are not limited to, Synthetic Air Microjet cooling³, Micro Capillary Pumped Loop⁴, Silicon Microchannel Cooler⁵, etc. Most of these innovative cooling solutions require far less operating power, fewer or no mechanical parts, and smaller components. These cooling devices are governed by basic principles of heat transfer using phase change, conduction and convection.

1.2 Electrowetting and Electrowetting on dielectric (EWOD)

With reference to the way in which the cooling medium is handled for cooling, Electrowetting on dielectric⁶ (EWOD) is one concept which has been recently developed and holds promising capabilities amongst all the above technologies for the future of electronics

cooling. Electrowetting involves changing the wetting ability of a drop by using electric field, especially on hydrophobic surfaces, hence making droplet manipulation easy. The reason we use hydrophobic surfaces as the platform for EWOD is obvious due to the fact that the wetting enhancement by using electric field is unidirectional, i.e., we can only decrease the surface

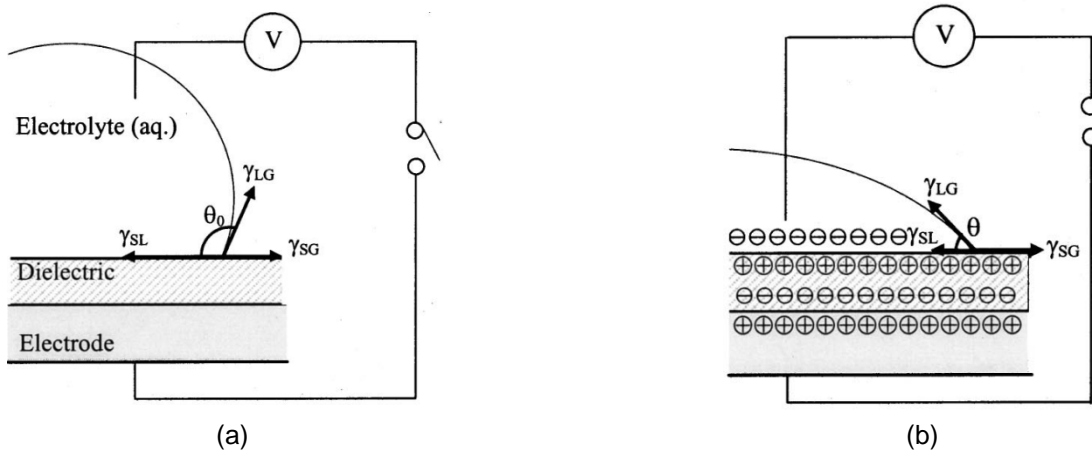


Figure 1.1 EWOD effect⁶ on a hydrophobic surface showing the drop before (a) and after (b) applying electric field.

tension (or improve the wetting ability) by the application of electric field and not vice versa.

Referring to Figure 1.1(a), a drop (electrolyte) placed on a hydrophobic surface takes the shape as shown. γ_{LG} , γ_{SL} and γ_{SG} is the surface tension between the liquid-gas, solid-liquid and solid-gas interface respectively. The angle between γ_{LG} and γ_{SL} is defined as the contact angle θ_0 , and is the parameter of focus in this section. The EWOD phenomenon occurs when an electric potential is applied as shown in Figure 1.1(b). Due to this electric field, the charges within the liquid drop and the solid dielectric are re-distributed into opposite charges, thus modifying the surface energy at the solid, liquid and gas interface. This develops repulsive forces between the like charges within the drop and decreases the net surface tension by reducing work done in expanding the surface area of contact. This in turn, decreases the contact angle, θ_0 . Another observation to make is that due to the re-distribution of charges between the interfaces, an electrostatic force between opposite charges facilitates the drop to

move radially outward. This is the driving force to facilitate easy manipulation of the drop as explained in sub-section 1.2.1.

The theoretical analysis of electrowetting is discussed in detail in various papers^{7, 8, 9}. The basic theory is governed by the Lipmann equation¹⁰ which gives us the relation between the surface tension γ and the voltage V applied

$$\gamma = \gamma_0 - \frac{1}{2}cV^2$$

where γ_0 is the surface tension at the solid and liquid interface when the circuit is open i.e., when no charge is present, and c is the capacitance of the dielectric layer. The above equation can be expressed in terms of the contact angle θ_0 by using the Young's equation

$$\gamma_{SL} = \gamma_{SG} - \gamma_{LG} \cos \theta$$

then we have

$$\cos \theta = \cos \theta_0 + \frac{1}{\gamma_{LG}} \frac{1}{2}cV^2$$

where θ_0 is the contact angle when no voltage is applied. This is the basic principle which has been used to transport a drop or coolant from one spot to the other on the microfluidic device for hotspot cooling.

1.2.1 Microfluidic Hotspot Cooling Device using EWOD Principle

There have been many successful attempts by various research groups to build and operate microfluidic devices for electronic hotspot cooling. Pamula et al^{11, 12}, Oprins et al¹³, Baird and Mohseni¹⁴ were some of the researchers who have worked on these devices which involved moving the coolant drops using EWOD principle across artificially created hotspots on patterned circuits. Figure 1.2 shows the phenomena of droplet transportation using EWOD with the drop sandwiched between two devices with the patterned circuits (shaded dark) while the top circuit controlling the motion of the drop and the bottom serving as the hotspot with the help of a small heater. Figure 1.2(a) through 1.2(d) shows a cool drop moving over the hotspot with the help of EWOD, the heat being transferred to the drop through heat transfer, the hot drop

moved away from the hotspot leaving behind a cooled spot. This process can be repeated by using multiple drops, one behind the other, to achieve continuous cooling effect.

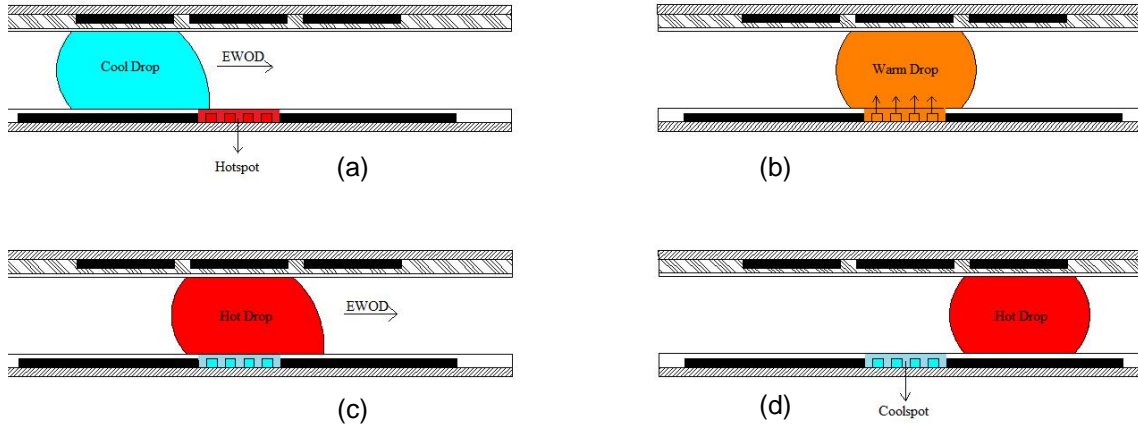


Figure 1.2 Concept of hotspot cooling by EWOD ((a) through (d)) showing heat removal by the cool drop.

1.3 Ionic Liquids (IL's)

Ionic liquids¹⁵ (IL's) are salts in liquid form at room temperature and are also referred to as Room Temperature Ionic Liquids (RTIL's). They are prepared¹⁶ by the combination of cations and anions producing liquids that have unique properties like low or negligible vapor pressure, good thermal stability, inflammability and are chemically inert to most of the known materials.

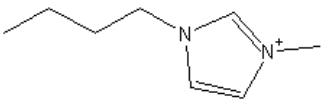
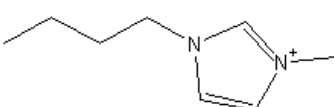
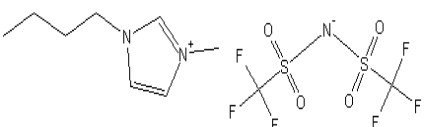
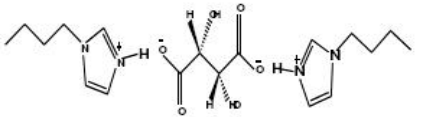
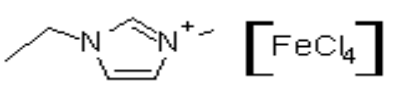
1.3.1 Ionic Liquids for Electronic Hotspot Cooling

In the past, Electrowetting has been performed on various liquids, popularly on water based electrolytes. However, due to their physical and chemical properties like low thermal stability, high vapor pressure and tendency of corrosion to metals, there arose the need to use special liquids, like IL's, which met our requirements. In the device for hotspot cooling, different IL's were used for EWOD and subsequently, as coolants for hotspot cooling device. In Table 1.1, relevant details of the IL's which were used for the device is given. They were chosen based on the availability and some special properties like colorless appearance, hydrophobicity, low viscosity and saturation voltage under EWOD. Colorless IL's made the visualization of temperature change of the hotspot easier as Liquid Crystals sensitive to temperature were painted behind the device. Low viscosity of the liquid meant faster EWOD movement and higher

cooling ability. High saturation voltage meant operation at higher voltages and this also gave better EWOD motion.

It has to be noted that the numbering of the IL e.g., IL1, IL2, etc., was purely for convenience sake. It did not change the structure or the chemical name.

Table 1.1 Structures of Ionic Liquids used with some properties

No.	Acronym	Chemical Name	Structure	Special Properties
1.	[bmim][Cl] or IL1	1-butyl-3-methylimidazolium chloride		Colorless, good hydrophobicity
2.	[bmim][Br] or IL2	1-butyl-3-methylimidazolium bromide		Colorless, good hydrophobicity
3.	[bmim][NTf ₂] or IL3	1-butyl-3-methylimidazolium bis(trifluoromethylsulfonyl)imide		Colorless, low viscosity
4.	[bmim] ₂ [Tartrate] or IL4	bis(butylimidazolium) tartrate		Colorless, high saturation voltage but bad hydrophobicity
5.	[emim][FeCl ₄] or IL5	1-ethyl-3-methylimidazolium iron (iv) chloride		Colored but very low viscosity

All the above RTIL's were used for the hotspot device for cooling, except for IL4 and IL5. In case of IL4, controlling the volume of the drop dispensed on the chip was difficult due to its bad hydrophobic nature and for IL5, its dark orange color made it incompatible for LCT.

1.3.2 Electrowetting Experiments on IL's

As mentioned in section 1.2, electrowetting involves changing the wetting behavior of a liquid drop by applying electric voltage. The voltage applied can be unidirectional (DC voltage) or bidirectional (AC voltage). Here, electrowetting was performed on all the IL's, as noted in Table 1.1, with AC voltage for comparing the results with that of DC voltage reported by Yasith

et al¹⁷. It was noted that AC electrowetting gave better results by improving droplet transportation which was attributed to frequency effects¹⁸ and conductivity effects¹⁹. In the present section, contact angle measurement using a goniometer is explained.

Figure 1.3 shows the experimental setup. The goniometer (CAM 101, www.ksvltd.com, Monroe, CT) consisted of an XY stage, a holder, light source and a CCD camera. The camera

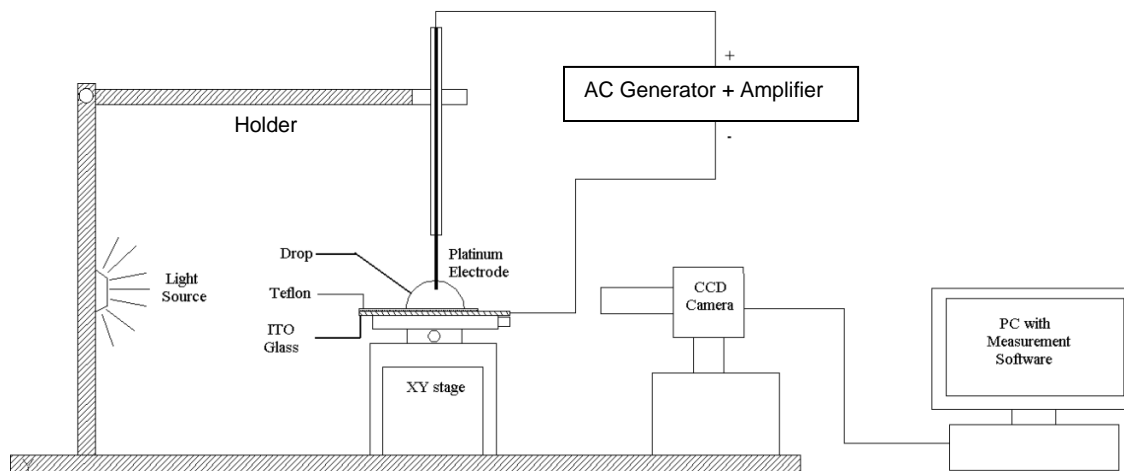


Figure 1.3 Experimental setup of contact angle measurements of IL's using goniometer.

was connected to a PC installed with measurement software called CAM 200. The drop was placed on an amorphous fluoropolymer (Teflon) coated 30 nm thick Indium-Tin-Oxide (ITO) pre-coated glass slide (purchased from Delta Technologies, Still Water, MN) on the XY stage. The Teflon solution was prepared by a mixture of 4% (w/v) Teflon AF1600 (DuPont, Wilmington, DE) and fluoroinert FC75 solvent (Fisher Scientific, Barrington, IL). A platinum wire (anode) was dipped into the drop and the ground was connected to the bare ITO on the glass slide. The ends were connected to a waveform generator (Agilent 33220A) which used an amplifier (TREK Model PZD 350). CAM 200 has the ability to grab the images off the camera and perform image processing to get the contact angle of the drop under applied voltage. For every IL drop, voltages were ranged from 0 V to its corresponding saturation voltage. The saturation voltage is defined as the voltage at which the dielectric reaches its highest charge storing capacity.

Beyond the saturation voltage, the dielectric breaks down and behaves as a conductor. In the next section, the results of the EWOD experiments with the IL's considered are presented.

1.3.3 AC EWOD Curves for IL's

An EWOD curve represents a plot between the contact angle (CA) of the drop versus the voltage (V) applied. An ideal curve is shown in Figure 1.4 in which it is desirable to have the curve take the path along the red dashed line which shows the decreasing contact angle for

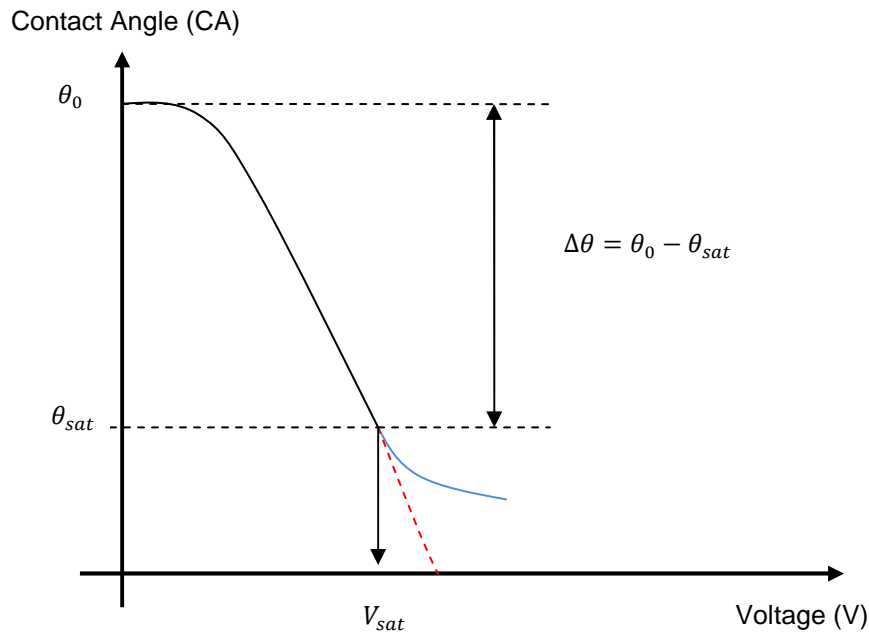


Figure 1.4 An ideal EWOD curve showing the actual trend in blue and desired in red. increasing voltage, but in reality, the actual curve takes the path of the blue line. This is because of saturation effects and dielectric breakdown as explained in the previous section.

The saturation voltage V_{sat} varied from liquid to liquid. In case of RTIL1 and RTIL2, V_{sat} was larger than that of RTIL5 and in case of RTIL3, the value was larger than that of RTIL1, RTIL2 and RTIL5, combined, which could be related to the cationic effects¹⁸ in the IL's. Of all the IL's RTIL4 had the lowest CA at V_{sat} .

Figure 1.5 shows the EWOD plots between AC and DC (DC data provided by Yasith et

al¹⁷) voltages of all the IL's tested and also shows the plot for De-ionized water (used for

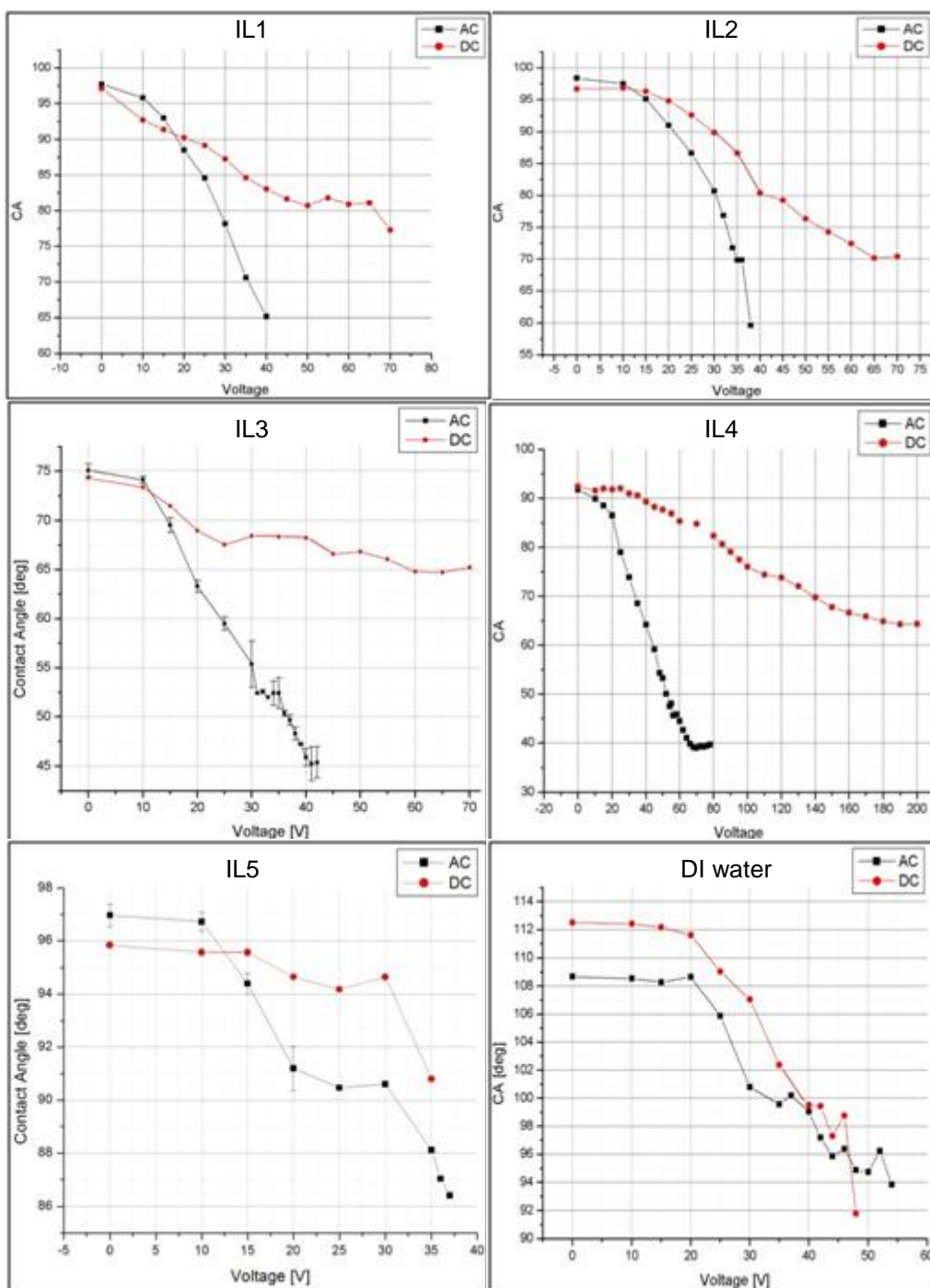


Figure 1.5 EWOD curves of all the liquids tested. IL3 and IL4 have the best results.

comparison). From the plots, we can see a clear difference between the two, with the AC giving lower contact angles for smaller voltages. It has to be noted that the experiments were performed at a constant frequency of 1 KHz and under the same experimental setup.

For the microfluidic hotspot cooling device, the performance of the IL's relies on the AC electrowetting properties as described above. In the next chapter, a detailed description of the device is given.

CHAPTER 2
DIGITAL MICROFLUIDIC DEVICE
2.1 Device Setup

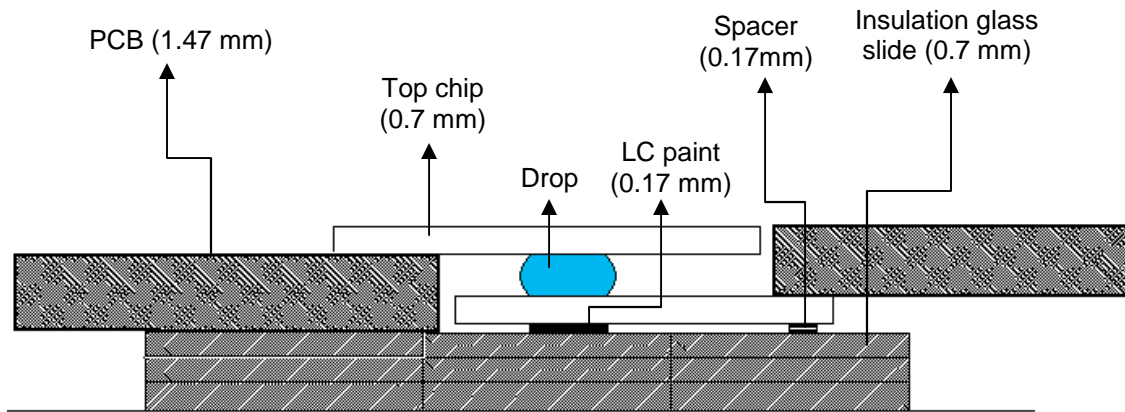


Figure 2.1 Cross section view of microfluidic device for hotspot cooling with the corresponding thickness.

The microfluidic device for hotspot cooling used the phenomena of AC EWOD to pump coolant drops across hotspot created on the device. Figure 2.1 shows the cross section view of the device which consisted of two glass devices or chips with patterned circuits on each of them. The circuits on the glass chips were connected to a copper clad Printed Circuit Boards (PCB) with the help of an electrically conductive adhesive transfer tape (3M, www.3m.com). The PCB's were further connected to Data Acquisition (DAQ) hardware, which was in turn connected to a computer which controlled the EWOD motion automatically, with the help of LabVIEW software. A detailed description of the hardware and software used is explained in section 3.1. The top chip consisted of the EWOD circuits required to move the drop while the bottom chip had the ground and the heater electrode, between which the drop was sandwiched.

In order to measure the temperature of the hot spot, it was difficult to incorporate a thermocouple, given the space and dimensions constraints. Therefore, Thermochromic Liquid Crystals (TLC) paint, or LC's sensitive to temperature, was used to visualize the temperature change by interpreting the change in color to temperature. When the LC's were painted below the hotspot, different color bands were observed and the temperature could be determined using Liquid Crystal Thermography (LCT). In the above setup, the heater was between the drop and the LC paint. Section 4.1 deals with LCT in detail.

In Figure 2.2, a setup of the device has been shown. The top and bottom chips were manufactured on standard 1016 mm (4 inch) diameter and 0.7 mm thick Indium Tin Oxide (ITO)

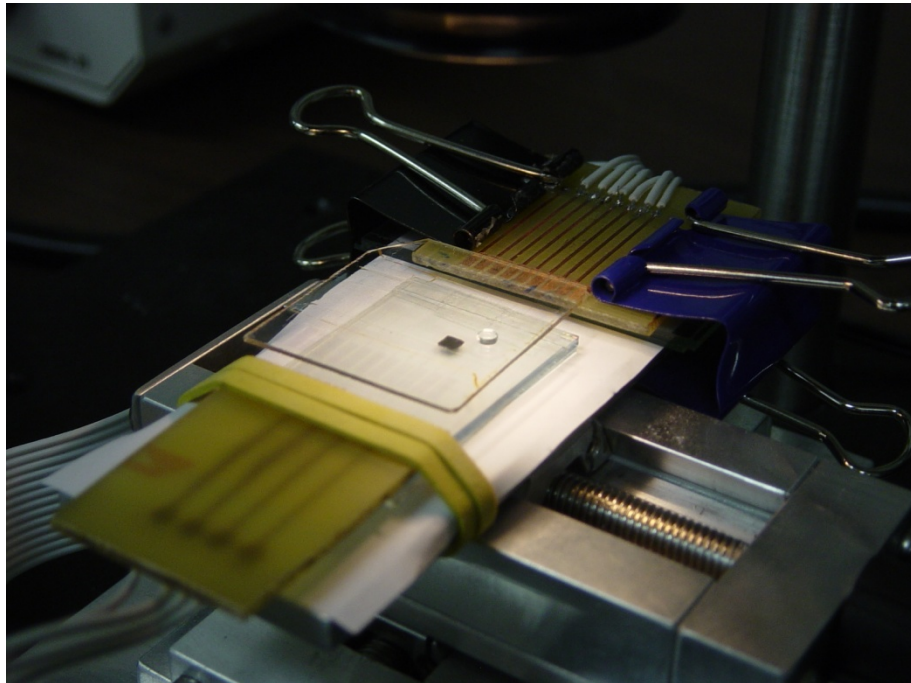


Figure 2.2 Figure showing the isometric view of the hotspot cooling device.

coated glass wafers (TechGophers Corp., CA). ITO is a new material used in the field of electronics which is transparent in appearance and is sometimes used in place of standard copper conductors, especially for applications which require better visibility of devices placed under each other. In the present case, ITO not only served as a good electrical conductor but

enabled us to see the chips placed below. The ITO circuits were fabricated using standard microfabrication techniques as explained in section 2.3.

The PCB interfaced the connections from the DAQ system to the top and bottom chips. Unlike copper, it is very difficult to solder any conducting material onto ITO terminals directly.

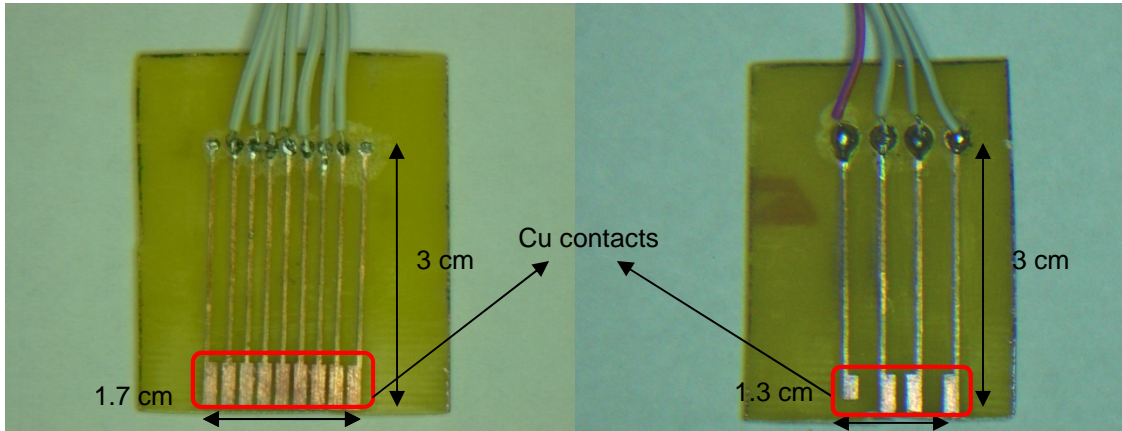


Figure 2.3 Top chip PCB showing the etched copper electrodes.

Therefore, conductive adhesive tapes were used to attach the ITO terminals on the chip to the copper terminals on the PCB. As shown in Figure 2.3, the circuit on the PCB was fabricated by printing the design on a photographic paper and then pressing it firmly on the copper clad PCB while applying heat. The paper was slowly peeled off from the PCB with the help of soap solution to reveal the mask of the design, which was then dipped in a copper etchant (Ferric Chloride solution, MG Chemicals, Canada) to etch the area surrounding the mask, leaving behind the desired pattern.

In the next section, a detailed note on the chip circuit and PCB circuit, right from design to development, is given. It has to be noted, that throughout the development of the device for hotspot cooling, many designs were considered, fabricated and used on the ITO chips and changes were made constantly to improve the performance of the device. The next section deals with the final design which was found to give the best performance in terms of the speed of the drop and the heat removal from the hotspot.

2.2 Heater and EWOD Circuit Designs

The circuit designs that were used for the hotspot cooling device were created using Tanner EDA's (www.tanner.com) L-Edit software. The finished circuit designs were exported to

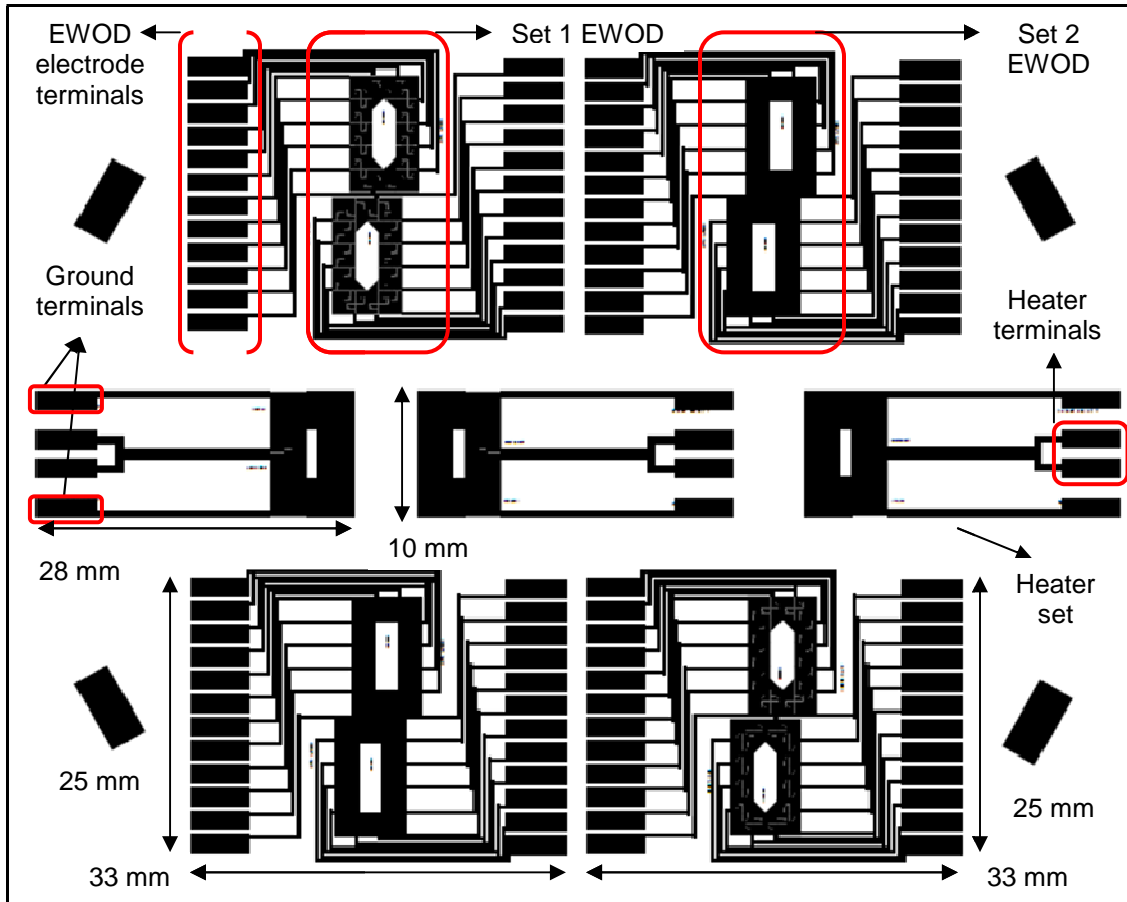


Figure 2.4 Mask showing two EWOD sets and one heater set used in photo lithography for cooling device fabrication.

GDS (Graphic Data System) file type and were then converted to PostScript (PS) format using LinkCAD software (www.linkcad.com). The PostScript format allows us to view the final design of the circuit which is similar to PDF format. The PS file was sent to a mask printing company, CAD/Art Services Inc. (www.outputcity.com) for use in photo lithography. Photo lithography is a microfabrication process which is explained in detail in section 2.3. The mask which was printed and used for patterning the circuits on the top and bottom chips is shown in Figure 2.4. This

mask shows three sets of patterns, two sets for the EWOD chip and one set for the bottom or heater chip. Another copy of the EWOD chip designs were printed on the other side of the heater designs so that maximum real estate on one ITO glass wafer was used. For efficient fabrication, each EWOD design had two chips within it, enabling us to use both sides of the chip for two different liquids.

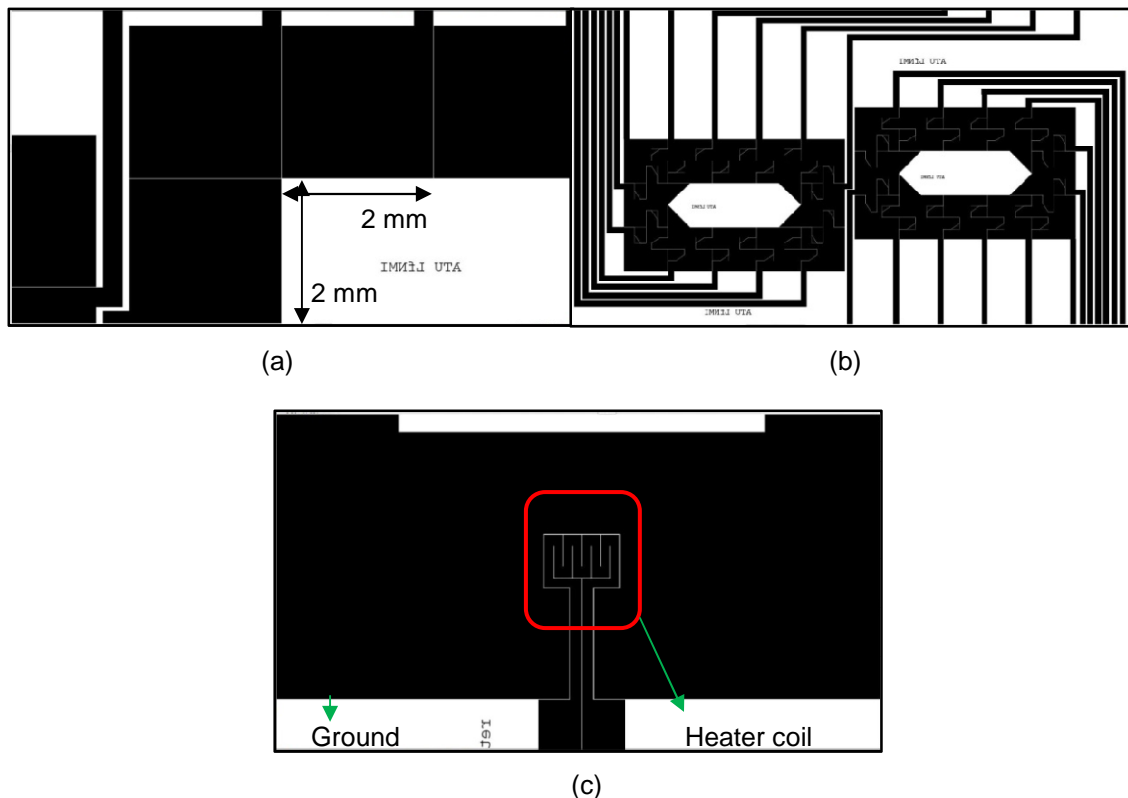


Figure 2.5 Set 1 (a) and set 2 (b) EWOD designs with heater (c) set.

Figure 2.5(a) through 2.5(c) shows the above mask with the set 1 EWOD chip design, set 2 EWOD chip design with inter-digitating finger like electrodes and the seven-coiled heater design. These EWOD chip designs were built after multiple changes of the design parameters. These changes included the electrode pad size, spacing between the top and bottom chips and the drop size. Drop properties like heat removing capacity, viscosity and the electrowetting characteristics also fuelled the need to change designs.

As shown in Figure 2.5(a), the size of the EWOD pad was set at 2 mm with a gap of 0.01 mm between the pads, which was found to be ideal for the size of the hot spot generated by the heater. In Figure 2.5(b), the finger like structures protruding into adjacent pads was meant to enhance the motion of highly viscous liquids like IL1 and IL2. As the viscosities of IL1 and IL2 are high, it was observed that the drop lost contact with the next electrode pad and thus, the motion was broken. To counter this problem, these protrusions were made so that the drop always remains in contact with the next electrode. Smooth motion of the drop was also observed when the gap between the top and bottom devices was set at 0.6 mm.

The seven-coiled, 1.5 K Ω heater was designed in such a way that it lied directly in the path of drop. The area surrounding the heater, the ground electrode, was not connected to the heater electrode and maintained a constant gap of 0.01 mm. This meant there were two separate connections on the bottom chip, one which operated the heater and the other providing the grounding for the EWOD circuit.

2.3 Device Fabrication

The fabrication steps involved basic clean room MEMS fabrication processes like spin casting, photo lithography, developing, etching and baking. Prior to any fabrication process, a detailed cleaning process was done which involved washing the wafer with Acetone, Methanol and then rinsing it with de-ionized water. The wafer was baked at 150°C on a hotplate (Isotemp, Fisher Scientific) to dehydrate it completely.

As the name suggests, spin casting involves depositing thin films of uniform thickness on substrates by spinning them. Thin film deposition included two materials, Hexamethyldisilazane (HMDS), a colorless solution used to enhance the adhesion of photoresist (PR) to the wafer, and the PR itself, a material sensitive to light. Referring to Figure 2.6, HMDS was poured and spun on a vacuum chuck at a custom recipe. The recipe involved spinning the wafer to 500 RPM for the first 5 seconds and then ramping it up to a speed of 4000 RPM at a rate of 900 RPM/sec. The wafer was spun for the next 30 seconds at this constant

speed. After depositing HMDS, the wafer was baked at 150°C for 1.5 minute. The same spinning recipe was used for depositing PR on the HMDS layer, after which, the wafer was

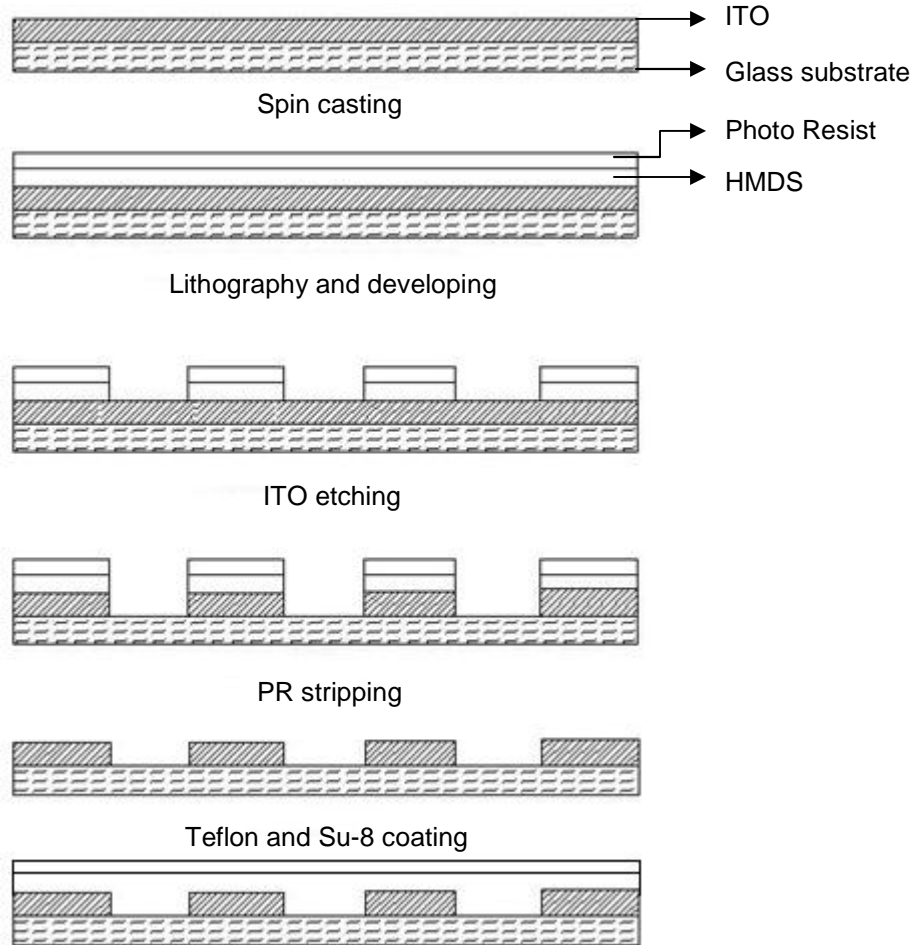


Figure 2.6 Figure showing the fabrication process.

baked again at 115°C for a minute. After spin casting process, photo lithography was done.

Photo lithography is used to selectively remove parts of the PR. This is possible with the help of a lithography mask. As shown in Figure 2.4, the mask contained a dark pattern of the circuit to be printed on the wafer. When the wafer was subjected to high energy ultraviolet (UV) rays, the light passed through the blank portions on the mask and did not pass through the printed portions. This changed the chemical properties of the PR (sensitive to light) in only those regions on the wafer which were subjected to UV rays. After lithography, the wafer was baked

at 115°C for a minute to harden the PR untouched by light. The next step involved developing the processed PR.

A Developer solution (MF-391, ROHM and HAAS) was used to dissolve and remove parts of the PR which was exposed to UV rays, leaving behind the unexposed PR which formed the pattern and exposing the ITO layer. In order to make the unexposed regions on the wafer impervious to the effects of etching, baking was done to harden them.

Post developing and baking, etching was done to remove the ITO layer unprotected by the PR. The etchant used was a mixture of HNO₃, HCl and de-ionized water in the ratio of 1:8:15 respectively. The duration of etching was 5 minutes. To catalyze the etching, a constant temperature of 55°C was provided to the etching solution. Finally, a PR stripper solution was used to remove the baked PR to reveal the chip with the ITO patterned circuitry.

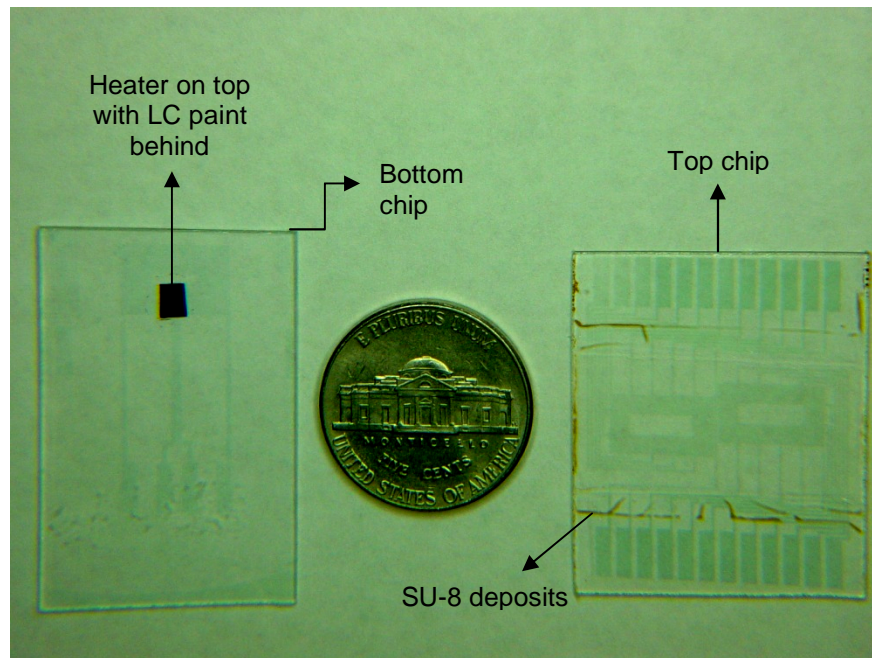


Figure 2.7 ITO patterned bottom and top chips compared to a 5 cent coin.

The wafer with the ITO patterns was diced into smaller chips along the sets of EWOD and heater designs. Figure 2.7 shows the diced chips with the ITO circuits. The diced chips were then ready for the next step in fabrication process – to deposit the dielectric layer. SU-8²⁰,

a photoresist used for high aspect ratio lithography, was used as the dielectric layer. In order to spin cast a 5 μ thickness SU-8 layer, the wafer was initially ramped up to 500 RPM at 100 RPM rate and spun for the next 5 seconds. Next, it was spun to a speed of 3000 RPM at 300 RPM ramp rate for the next 30 seconds. After spinning the SU-8 onto the wafer, it was baked on the hotplate at 65°C for one minute and then at 95°C for 3 minutes. The wafer underwent lithography, with the entire surface exposed to UV rays. This polymerized the SU-8 layer.

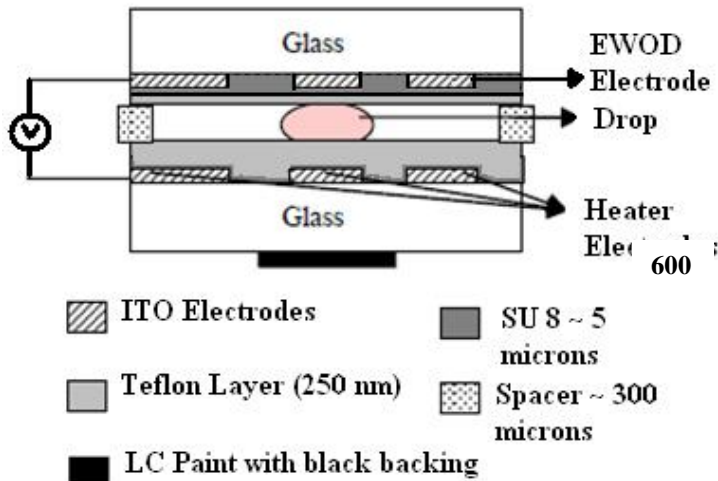


Figure 2.8 Cross section of the top and bottom chips after fabrication.

The wafer was again heated at 65°C and 95°C each for one minute and then at 150°C for 15 minutes, concluding the SU-8 deposition process. In order to achieve hydrophobic surfaces on the active sides of the top and bottom chips, amorphous fluoropolymer solution (Teflon) was spin casted as shown in Figure 2.8. The solution was prepared by mixing amorphous fluoropolymer crystals (DuPont) in a per-fluoro compound FC-75 solvent (Acros Organics) with a 2.5 w/v ratio. The recipe involved ramp up spin speed of 500 RPM at 100 RPM rate for 5 seconds and then 1000 RPM at 100 RPM spin rate for 30 seconds. This process was performed twice to yield a thicker Teflon layer. The chips were baked in an oven (Thermolyne Inc.) at 115°C, 150°C and 180°C for 10, 15 and 30 minutes respectively. Once the final device with the top and bottom chips was fabricated, it was ready for the hotspot cooling experiments, dealt with more details in the next chapter.

CHAPTER 3
EXPERIMENTAL

3.1 Hardware and Software

The setup for hotspot cooling device comprised various hardware and software components which initiated, controlled and recorded the motion of the drop. Figure 3.1

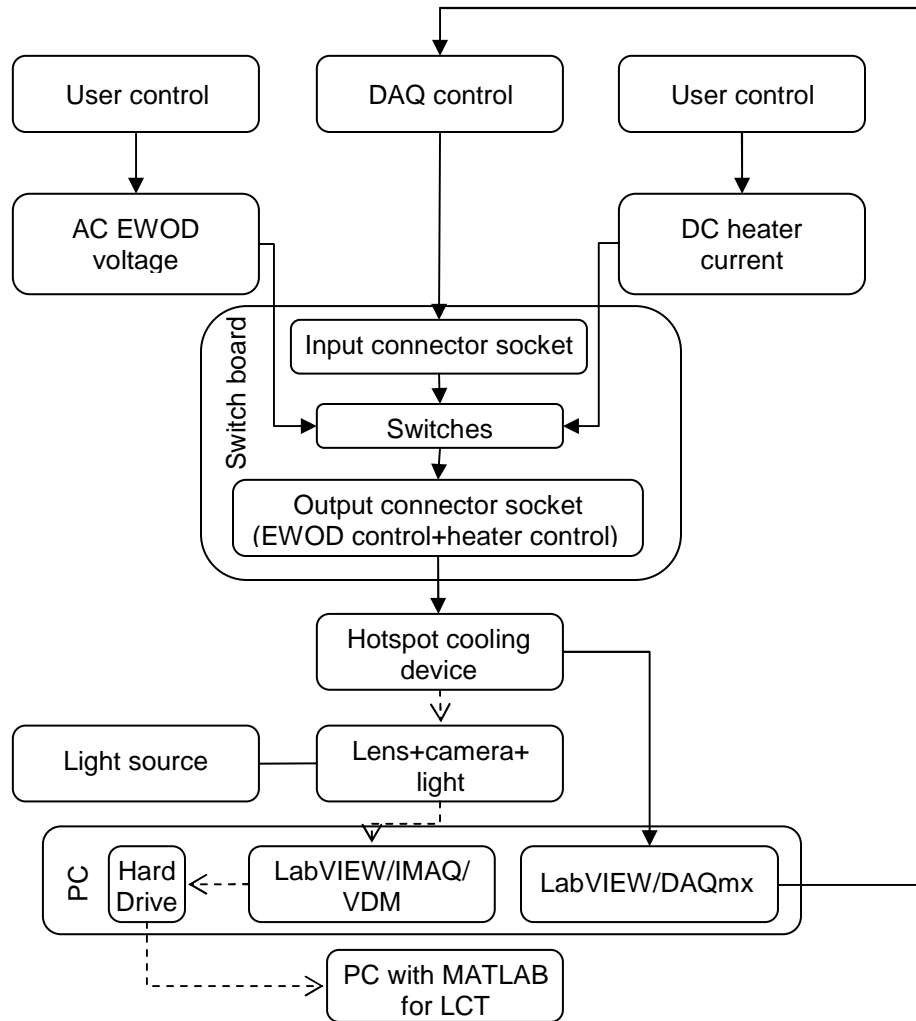


Figure 3.1 Flowchart showing the hardware and software components of the entire setup. Dark arrows represent digital and electrical signals while dotted arrows represent visual data.

shows a flow chart of the various hardware and software components of the microfluidic device for hotspot cooling. At the top of the flow chart, the waveform generator and the DC sourcemeter were directly controlled by the user. This was a onetime operation to set the AC voltage and DC current for the hotspot cooling device. The voltage and the current outputs were connected to a custom built switch board with switches, an input and an output connector socket. The input connector socket was connected to a DAQ system which comprised a digital I/O device (NI USB-6509), a connector block (NI SCB 100) and a cable (NI SH100-100-F) connecting the two. The connector block was connected to the input connector socket on the switch board with spare 40 pin IDE/ATA hard drive cables. The connections from the socket, AC and DC source were wired to the input side of the corresponding switch. As shown in figure 3.2, the switch board with the input and output connector sockets along with the EWOD and the

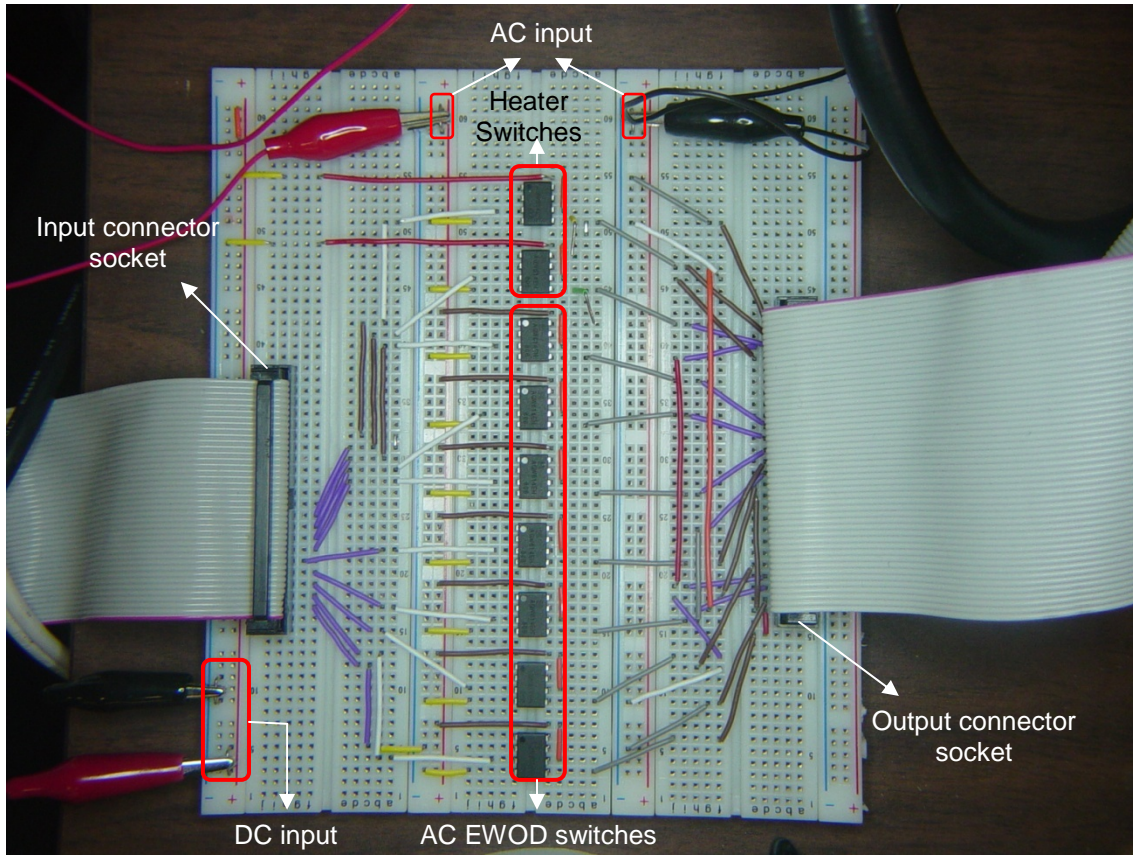


Figure 3.2 Custom built switch board showing the connector sockets and switches.

heater switches is shown. Seven AC EWOD switches corresponded to seven distinct EWOD pads on the top chip and two DC heater switches corresponded to the heater terminals on the bottom chip of the hotspot cooling device. Separate AC voltage and DC current lines were taken from the output side of the corresponding switch and wired to the common output connector socket. A 50 pin IDE/ATA cable connects the output connector socket to the hotspot cooling device. Directly above and normal to the device, a ring light, connected to a halogen lamp source (StockerYale IMAGELITE Model 20), a lens arrangement (Edmund Optics, VZM 1000 Video Lens) and a color CCD camera (HITACHI, KP-D20BU) are fixed with the help of a stand and stage arrangement. In order to capture the images off the CCD camera, a PCI interface frame grabber card (NI PCI-1411) was installed in the PC. The camera and the frame grabber were connected by an S-Video cable. The data from the hard drive was sent to another PC with MATLAB installed for LCT. In order to control the DAQ system, it was connected from the PC to the digital I/O device by a USB cable. This completes the hardware setup.

Figure 3.3, shows an overview of the setup used for the hotspot cooling device. To the

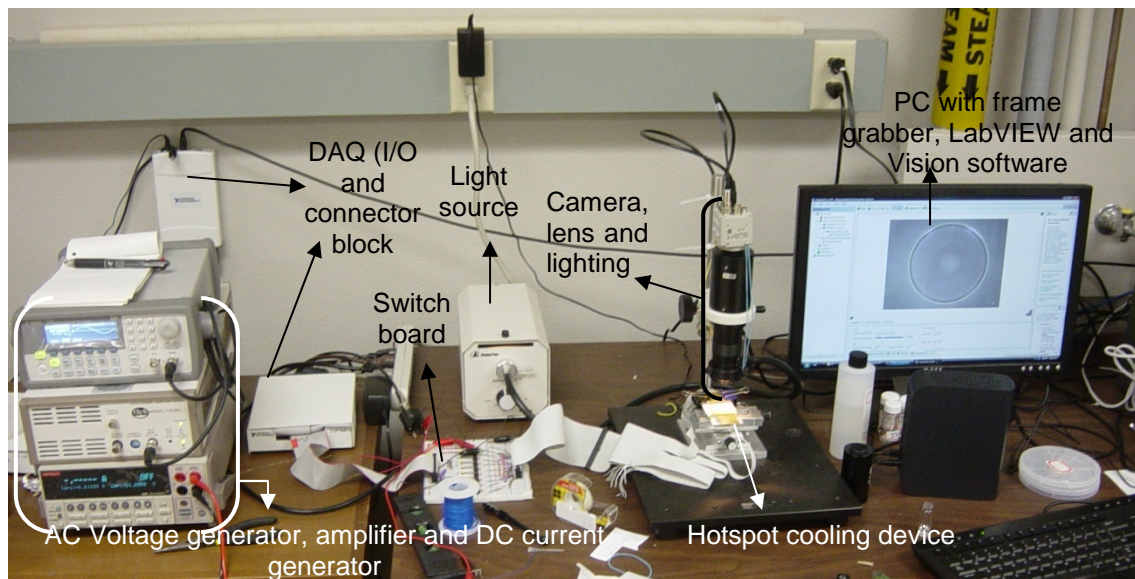


Figure 3.3 Overview of the hardware and software setup.

left of the figure, an AC waveform generator (Agilent, Model 33220A), voltage amplifier (Trek, Model PZD 350) and a DC sourcemeter (Keithley 2400 series) were arranged in a rack. For the EWOD circuit, the AC voltage (in mV) from the waveform generator is sent to the amplifier, from which the voltage range is amplified to 100 times (V). The terminals are connected to the switch board with the help of clip-on wires. For the heater circuit, two wires connect the DC sourcemeter to the switch board. A single IDE cable connects the output connector socket to the top and bottom chip on the hotspot cooling device, which is fixed on a stage with XY movement (Velmex, Inc.). Finally, the CCD camera is connected to the frame grabber card installed in the PC.

The softwares used in the experiments mainly included LabVIEW 8.5 to control the experiment and gather visual data for LCT simultaneously. LabVIEW used NI-DAQmx 8.7.1 drivers for controlling the DAQ system in conjunction with NI-IMAQ 4.1 drivers for initializing the frame grabber card and capturing data (images and videos) via CCD camera. For image processing functions, NI-IMAQ used NI Vision Assistant software, which is explained in detail in sub-section 4.1.1. MATLAB was used to perform LCT and is explained in detail in sub-section 4.1.2.

3.2 Experimental Procedure

To start with, the AC and the DC machines were switched on and the voltage and current values were set to the desired values respectively. In case of the AC generator, the voltage was set at $1.5 V_{rms}$ which was amplified to $150 V_{rms}$ in the amplifier. Similarly, the DC sourcemeter current was set to a constant 0.011 A. With a heater resistance of 1.5 K Ω , the voltage in the heater circuit was 16.5 V. The PC was switched on and LabVIEW software was started. Two different programs, one for DAQ control and the other for image acquisition, was opened. The light source for the device was switched on and set at the correct intensity.

Once the above operations were done, the next step was to sandwich the drop between the top and bottom chips. Using a dispenser (Eppendorf AG), a certain volume of the fluid was

taken into the dispenser tip and dispensed on the bottom chip in such a way that the drop lied in the path of the EWOD ground electrode. The drop was then sandwiched by the top chip and its size was kept to a constant diameter of 2.5 mm, as shown in Figure 3.4. If the size fell long or short of 2.5 mm, the volume of the drop was adjusted using the dispenser. Care was taken to align the top and bottom devices by observing the live image on the PC monitor.

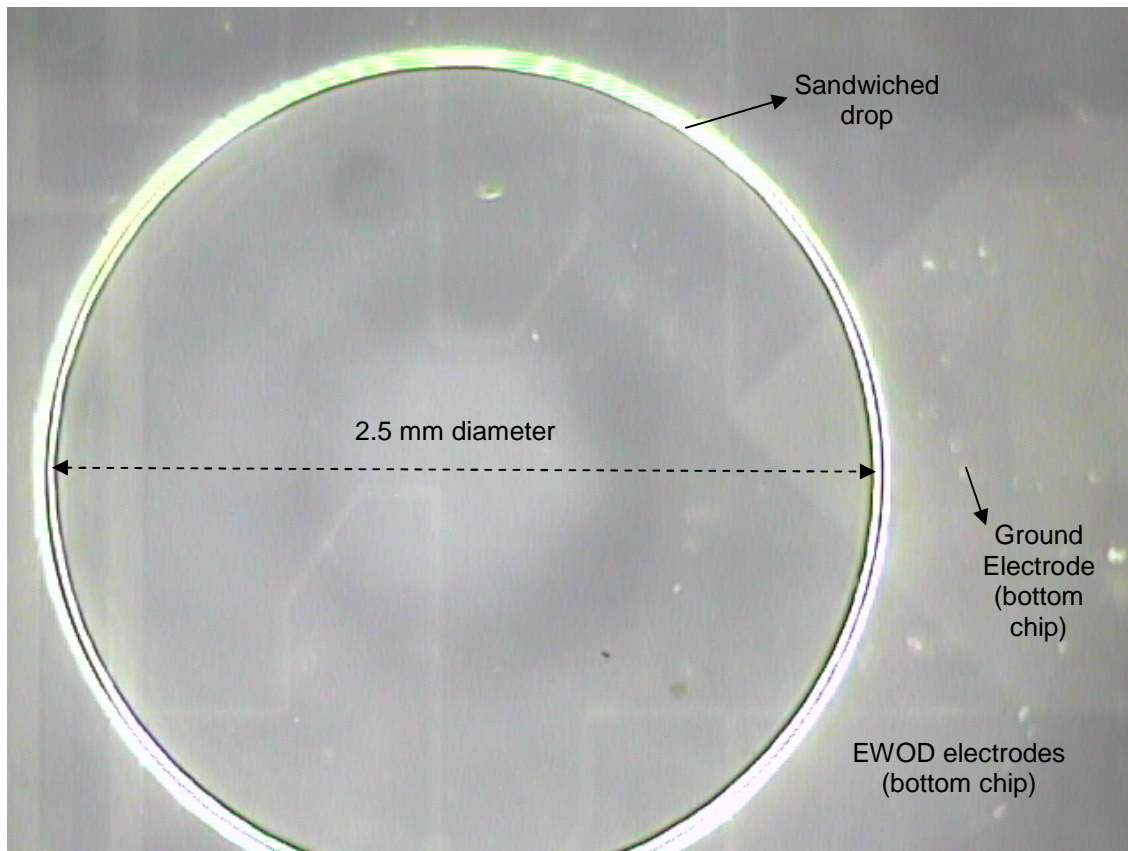


Figure 3.4 An RTIL1 drop sandwiched between the top and bottom chip, ready for the experiment. The ground electrode is slightly visible as its out of focus.

Once the drop was dispensed and sandwiched properly in the device, all attention was turned to the PC controlling the DAQ and the visual data acquisition. As mentioned before, two different VI's were used in LabVIEW, one to control the EWOD motion and the other to acquire the visuals. The VI which controlled the EWOD consisted of a switch on the front panel, which when turned on, sent signals to the digital I/O device through USB. The I/O device converted the signals into analog voltage signals not exceeding 5 V and sent it to the connector block. The

connector block had terminals which could be wired up to the switch board. In this case, only seven such terminals were needed to control seven individual EWOD electrode pads on the top

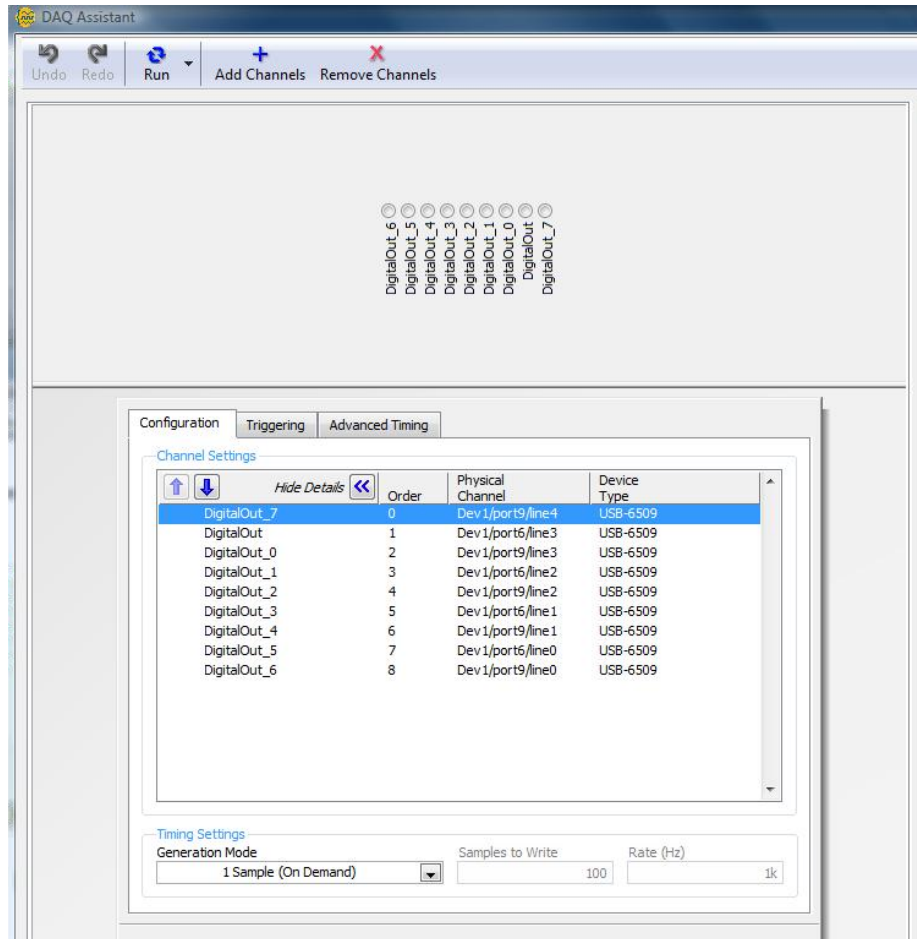


Figure 3.5 DAQ Assistant interface in LabVIEW showing nine ports assigned to the digital I/O device.

chip and two electrode pads on the heater switch, totaling to nine terminal connections from the connector block. Figure 3.5 shows the channels assigned in LabVIEW corresponding to the ports in the digital I/O hardware connected to the connector block. Similarly, every terminal in the connector block was wired to the corresponding switch on the switch board. Hence, by turning on the switch in the front panel, the signals were switched from one electrode to the next in the DAQ hardware and subsequently, on the switch board, hence moving the drop with the application of the external AC voltage. The EWOD VI also had a switching time input which

controlled the time gap between the switching of two consecutive electrodes. Considering the viscosities of the different liquid drops used, and after many trials, the switching time was set at 5 second.

The next step was to grab and record the images off the CCD camera and save it for LCT. These images contained the color of the LC paint when the drop was moved over it. For this purpose, the second VI, which was built to use the frame grabber card to record, snap and process the images, was used. Figure 3.6 shows the block diagram of the VI. To the left of the

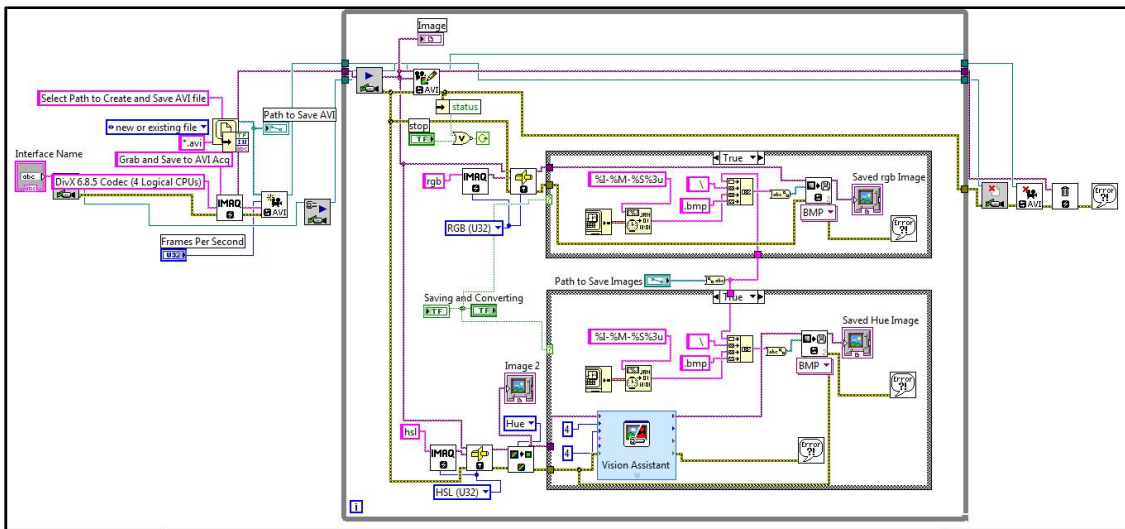


Figure 3.6 Custom built VI showing the block diagram for image acquisition and processing.

diagram, the program dealt with creating a path on the hard drive and store the visual data and initializing the frame grabber. The middle part enclosed in the loop added a frame to the video file, for every iteration performed. Notice the two loops within the main loop. The first loop captured individual frames from the main video stream when the image capturing switch was pressed and saved it in RGB format. The second loop captured frames and extracted the hue plane after storing the images in HSL format (section 4.1.1 explains more about conversion of RGB to Hue format for LCT). The Vision Assistant function played a role in processing the images. Finally, to the right of Figure 3.6, the data acquisition was terminated once the program

stopped. The images and videos stored were made available for final image post processing in MATLAB.

For LCT in MATLAB, the Image Processing Toolbox was used and a program was written to analyze the Hue images taken in LabVIEW and co-relate it with actual temperature. This was possible by using certain functions provided in the toolbox which calculated the pixel intensity value in the image and averaged them out to give a contour of different intensities in different regions of the Hue image. In order to relate pixel intensity in a Hue image to temperature, a thermocouple was used to note the actual values of the hotspot temperature corresponding to different color bands on the LC paint. This was calibrated and finally, a plot showing the temperature versus the corresponding color was constructed.

3.3 Data Collection and Organization

The visual data included images stored in RGB and HSL format and also videos created and saved in AVI format. The images were manually saved in LabVIEW by clicking the save button. The videos were recorded for the entire length of the experiment. The images in RGB and HSL formats were sent to MATLAB for LCT. The next chapter deals with the data handling and the analysis in detail.

CHAPTER 4

ANALYSIS AND RESULTS

4.1 Qualitative Analysis – Liquid Crystal Thermography (LCT)

Analysis of the visual data was divided into two parts. The first one pertained to qualitative analysis – results of which were an outcome of visual data. The second type of analysis was a numerical approach (explained in section 4.2) in which basic heat transfer relationships and actual device design values were used to calculate the heat power removed by the liquid drop, given the power applied to the heater. This section deals with the qualitative analysis called Liquid Crystal Thermography or LCT.

A brief outline of LCT was given in the previous sections. In LCT, a color image in RGB color space was converted to HSL (Hue/Saturation/Lighting) color space and the hue image was extracted. This hue image contained only the information pertaining to the true color of the pixel and not the saturation or the lighting. This helped us to better visualize a TLC image and demarcate the color bands to identify the temperature on the hotspot.

As explained in the device setup previously, it was difficult to incorporate a thermocouple directly in the path of the liquid drop to measure the temperature change on the hotspot due to the space and design limitations. Hence, a need arose to visually determine the temperature change on the hotspot by the use of Liquid Crystals or LC's sensitive to temperature, also known as Thermochromic Liquid Crystals²¹ (TLC's). When TLC's are subjected to temperature change, they emit colors within the visible spectrum. They have twisted molecular structures and are generally used in three forms, one in the unsealed form, second in the microencapsulated form and thirdly, in the form of printed sheets. TLC's in unsealed form are more susceptible to degradation as they can be easily attacked by dust, atmospheric gases and grease. They generally have a lifetime of few hours to days and are

mainly used for applications involving shear stress analysis and are not suitable for temperature measurements. Sealed TLC's are microencapsulated in polymers which protect them from the environment. They are sealed in tiny spheres of microencapsulation and are applied on surfaces by brush or spray paints. For the hotspot cooling device, this type of TLC was painted behind the heater of the bottom chip for hotspot cooling as temperature indicators.

As with any other temperature measurement method, LCT requires its own calibration. A plethora of literature works is available which describe the calibration method for LCT. LCT calibration²²⁻²⁴ involves controlling the thickness of the LC paint, the angle of the light source aligned with the LC paint and the spectrum of emission of the light source.

In order to obtain accurate change in color for a given temperature, the application of the LC paint behind the bottom chip was controlled in such a way that it was not more than 5 μ thick. This was controlled by spray painting the paint onto the glass surface. Apparently, while doing so, there were many voids created by air bubbles and this affected the quality of the color spectrum observed on the LC. To avoid this problem, the LC (R40C5W, LCR Hallcrest) was brush painted to a uniform size and dried for 20 – 30 minutes under an air blower. In order to visualize the color change better, a black backing paint (09-SPBB, LCR Hallcrest) was painted on top of the LC paint. The size of the LC paint was trimmed to the size of the hotspot. Figure 4.1 shows the LC paint and the hotspot. Note that the temperature decreased outward from the center with dark blue representing high temperature and red representing low temperature.

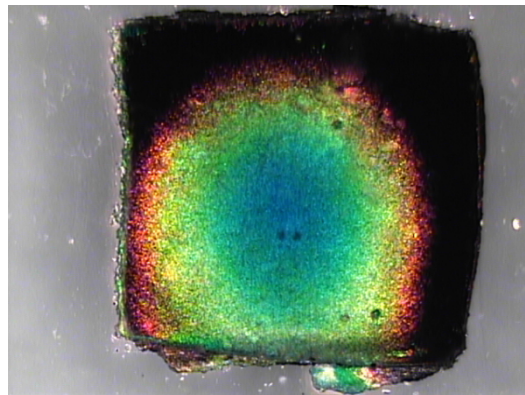


Figure 4.1 Figure showing TLC painted behind the glass creating a color contour when hotspot was switched on.

With reference to the lighting angle, the light source had to be positioned normal to the setup as the TLC was sensitive to viewing and lighting angles. Care was taken to ensure that there was no reflection from the surface of the top chip. This was very important as even slight amounts of reflection could add up to the pixel intensities of the RGB image and falsify results. The intensity of the light was also crucial as too low an intensity can give poor lit colors and too high an intensity could wash out the colors from the image. This was controlled by keeping the intensity constant throughout the experiments. The light source used here was a Tungsten halogen lamp which was found to be suitable for the LCT as it has only visible light emission spectrum and was free of UV or Infra Red (IR) light.

As shown in Figure 4.2, LCT was performed in three stages. Stage one involved conversion of the image TLC image from RGB color space to HSL/HSV/HSI image. This was done in LabVIEW by using NI Vision software. NI Vision consists of functions which perform

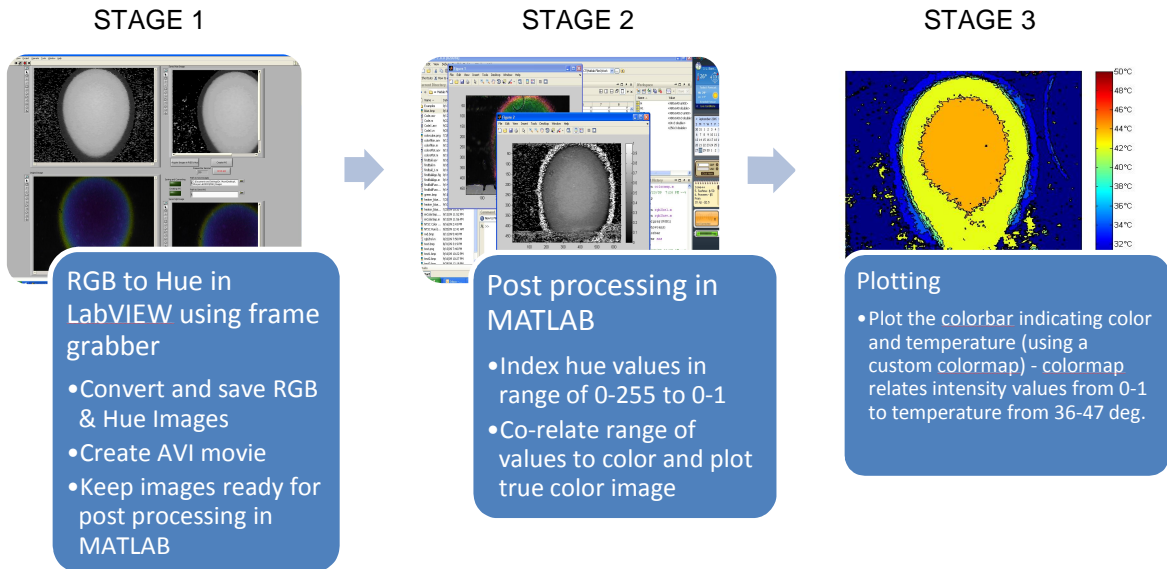


Figure 4.2 Figure showing the three stages in which LCT analysis was performed.

basic image processing tasks which can be wired directly in the block diagram of the image acquisition VI. Stage two involved pixel intensity calculations and correlating to temperature in MATLAB using the Image Processing Toolbox and stage three involved hue to true color

mapping, plotting colorbars and correlating color bands on the TLC to the actual temperature on the hotspot.

4.1.1 RGB to HSI/HSL/HSV Color Space Conversion using LabVIEW and NI Vision Assistant

Table 4.1 Pixel intensity combinations giving rise to various colors

Red	Green	Blue	Color
0	0	0	Black
1	1	1	White
1	0	0	Red
0	1	0	Green
0	0	1	Blue
1	1	0	Yellow
1	0	1	Magenta
0	1	1	Cyan
0.5	0.5	0.5	Gray
0.5	0	0	Dark Red
1	0.62	0.40	Copper
0.49	1	0.83	Aquamarine

Any image in RGB color space has information of the pixel values of three primary colors, i.e., red, green and blue. These values range from a combination of 0 to 1. If the R, G and B values in a pixel are set at 0, 0 and 0 respectively, then the pixel will be black. If the values are set at 1, 1, and 1, then the pixel will be completely white. Combinations of different pixel values between 0 and 1 gives rise to different colors. Table 4.1 illustrates the above explanation. For practicality, we can visualize each pixel to be a 3-D matrix with each matrix plane representing the values of each component of color, i.e., one plane with only R intensity values, the next with G intensity values and the third with B intensity values. The size of the

matrix is $m \times n$, where m represents the number of pixels in the X direction and n represents the number of pixels in the Y direction. $m \times n$ on the whole gives us the resolution of the image. For example, if the resolution of an RGB image is 640x480, then the image is interpreted to have 480x640x3 matrices of R, G and B values.

If we can find out the individual pixel intensity values of R, G and B, we get the color content in the image and hence, we can estimate the amount of color in any pixel on the TLC image. However, for LCT purposes, the RGB pixel intensities are not useful as every color has some proportion of white light. This can add up to the true color intensity and give us aberrant values. For this purpose, RGB data was converted to HSL/HSV/HSI color space, which stands for Hue/Saturation and Lighting or Value or Intensity. Lighting, Value or Intensity are

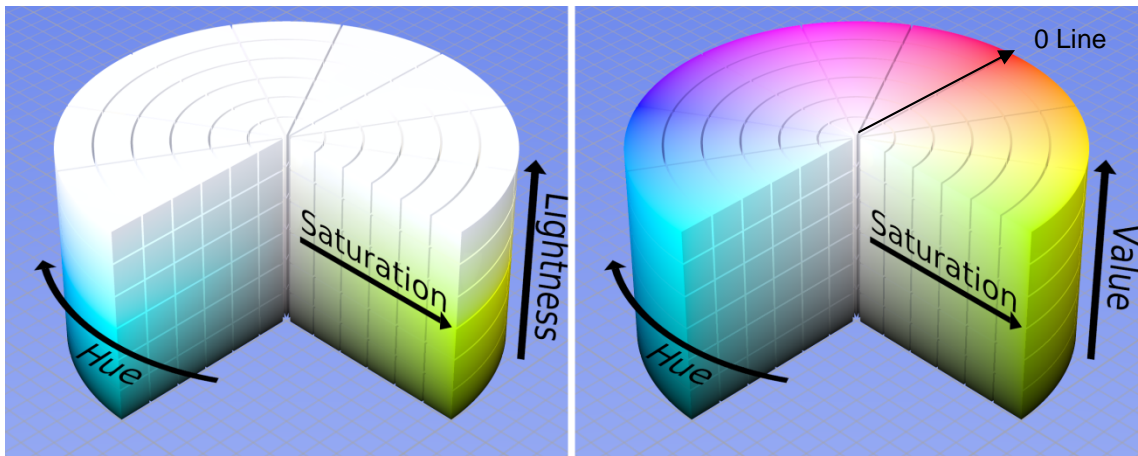


Figure 4.3 Figure showing the HSL and HSV color wheel. Hue is independent of lighting.

synonymous but vary by the way we represent them. Figure 4.3 interprets the HSI and HSL/HSV color spaces²⁵. It was observed that the hue component was independent of the lighting or value component. Hence, by converting a 32 bit RGB image to HSL color space, the lighting and saturation components were eliminated giving us an 8 bit grayscale image with only 1-D intensity values. These intensity values represented true color. The intensity values ranged from 0 to 255, around the HSL/HSV color wheel, with 0 given for red color (0 line) and 255 given for violet. Figure 4.4²⁶ shows the separated planes of an RGB image with its corresponding hue,

saturation and value components. The hue scale (0 to 360 represents angle on the color wheel) shows that red takes the lowest intensity value and is dark and blue color, the maximum and is bright in the hue image.

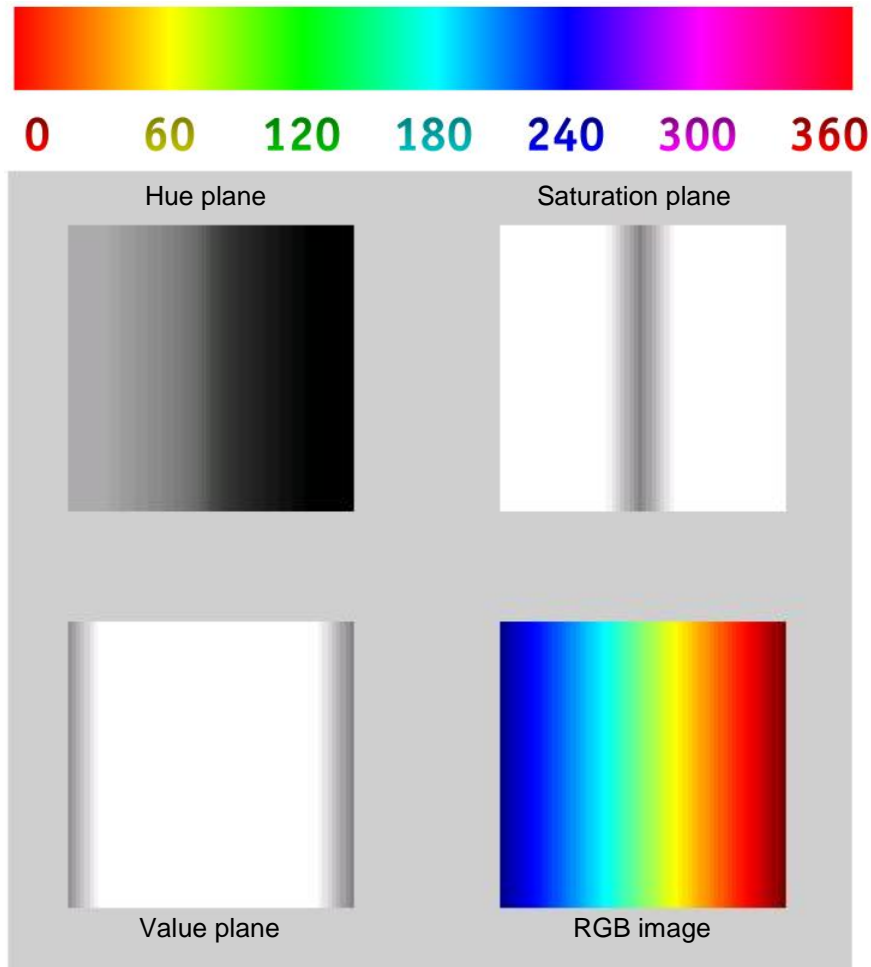


Figure 4.4 Separated color planes of an HSV image with the original RGB image and the angle of the color on the hue color wheel.

This concept was used in the image acquisition and processing VI in LabVIEW and the first results which were obtained was surprising. It was noticed that the outermost band in the hue image that relates to red was bright, contrary to what was stated before. This was due to the presence of pink color in the red band which made it take the highest value in the hue color wheel, resulting in a bright band, as shown in Figure 4.5. This problem could fixed by shifting

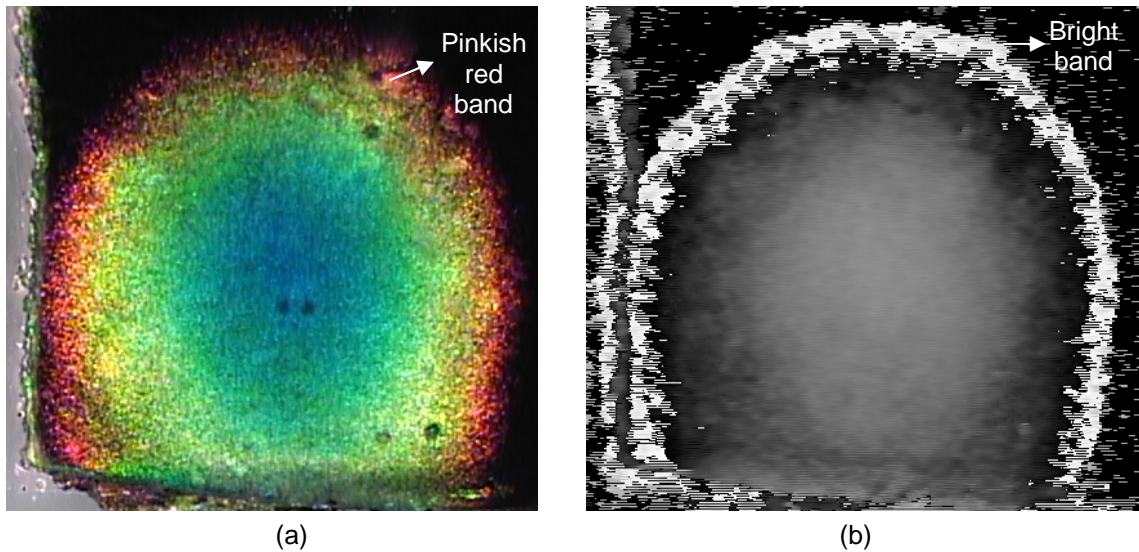


Figure 4.5 Error in RGB (a) to hue (b) conversion due to presence of pink color in the outermost red band in (a).

the 0 line in the hue color wheel to the lower side to include the pink pixel intensities close to 0.

Another way to tackle this problem, as shown in Figure 4.6, was to shift the RGB 0 line

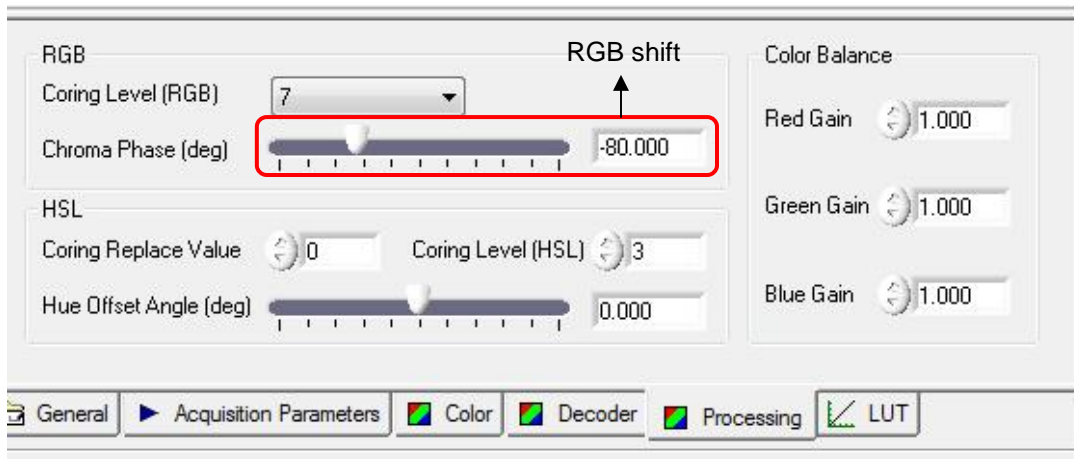


Figure 4.6 Phase shift of RGB line to a safe negative value.

to a negative value in the frame grabber itself. This ensured that all the variants of red color were included in the lower ranges of hue values, so there was no need to shift the 0 line of the hue color wheel. Figure 4.7 shows an RGB and hue image after the RGB color shift. Using this concept, the RGB images from the frame grabber card were converted to hue images without any errors. For this purpose, as mentioned before, LabVIEW was used.

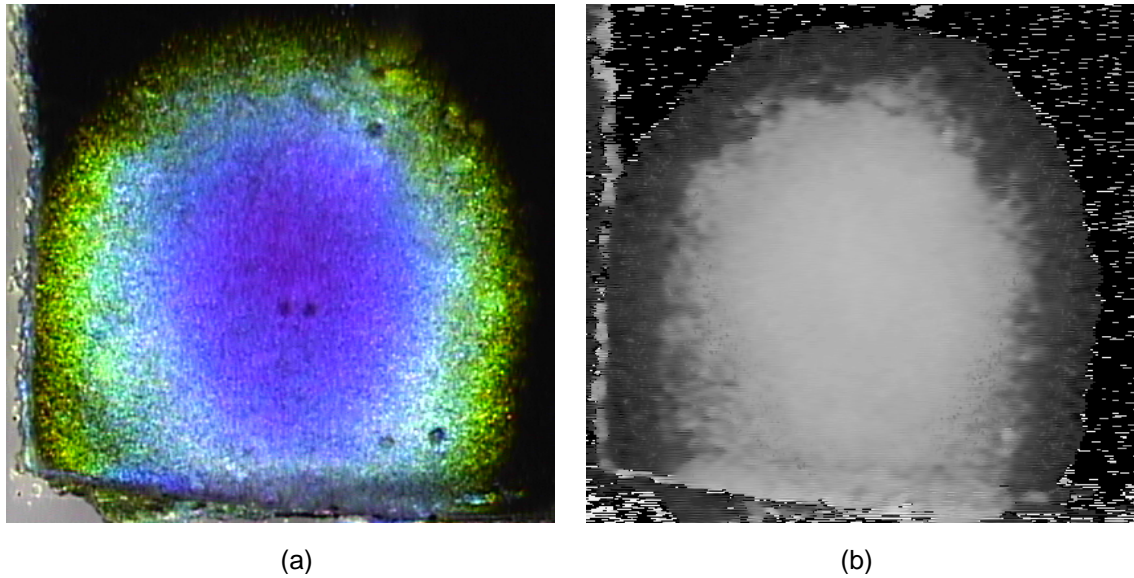


Figure 4.7 RGB image after the RGB shift (a) and the correct hue image with the red band showing the lowest intensity (b).

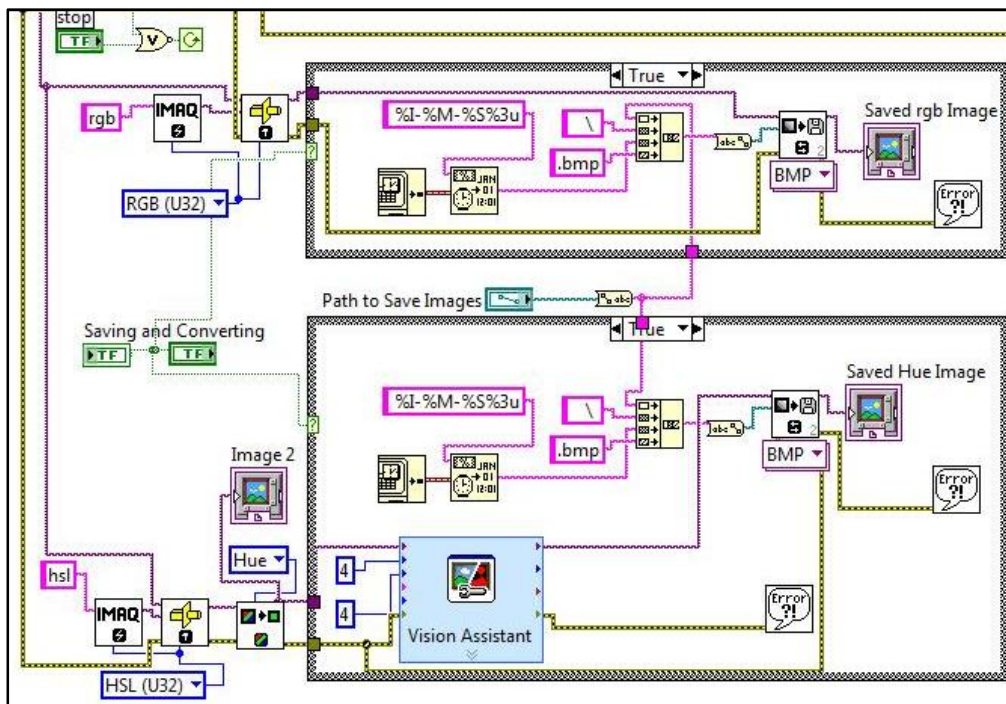


Figure 4.8 Custom built LabVIEW VI showing the different VI's used for RGB to HSL conversion and Vision Assistant VI for filtering.

Referring to figure 4.8, RGB signals (purple wire) were sent to a cast image VI (every block diagram is a set of VI's) set to HSL format. The HSL image was then sent to a color

component extraction VI which extracted the hue plane from the HSL image. Now, the image was sent inside a case structure for filtering. The filtering process was done only when the button to save the images was pressed. As mentioned before, this was a manual operation performed by the user. Filtering step was used to remove grainy spots from the image. The hue images were sent from the hue plane extraction VI to the vision assistant express VI inside the case structure. This VI used median smoothing to filter out the noise from the hue image. Figure 4.9 shows the images in hue, before and after filtering. The size of the filter represented the degree to which the filtering was done, without affecting the hue intensity values. The filtered images were saved in bitmap format and sent to MATLAB for LCT.

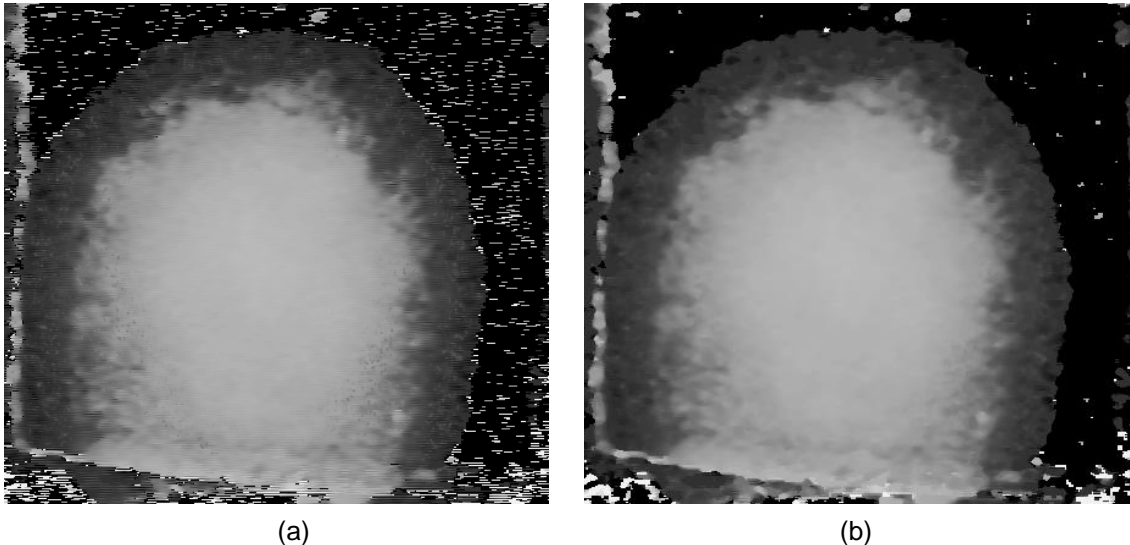
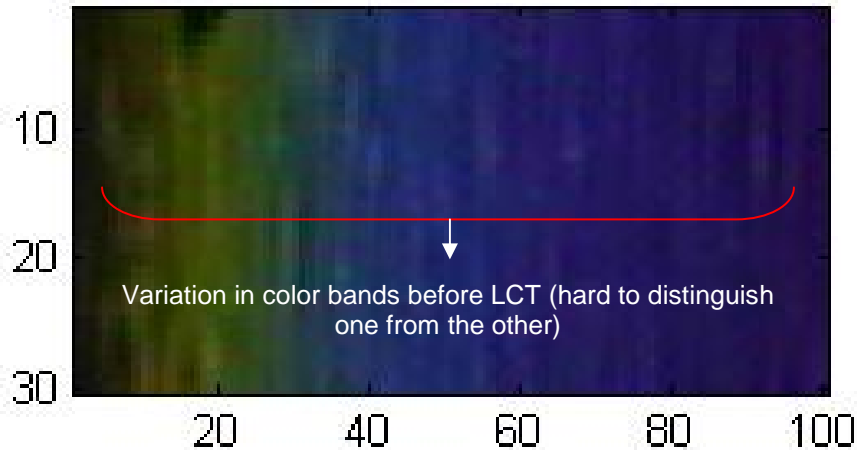


Figure 4.9 A hue image with noise surrounding the hotspot (a) and the filtered image with a considerable reduction in noise (b).

4.1.2 LCT using Image Processing Toolbox in MATLAB

The Image Processing Toolbox in MATLAB was used to perform LCT on the hue images. A MATLAB code was custom written to use the Image Processing tools. The images were read into MATLAB, the color map information was provided and contours were identified for changes in pixel intensities, relating to the changes in color bands on the original RGB image. These contours were then filled with colors that represent the temperature in those regions. Finally, a color bar was plotted which related the color to the calibrated temperature.

Referring to line 7 in APPENDIX A, the 'imread' command read the RGB.bmp image and saved it into the variable 'RGB'. RGB images were read in order to compare them to the final image after LCT. As explained in section 4.1.1, MATLAB read an image file and stored it as a matrix with $m \times n$ rows and columns which represented the resolution of the image. The information stored in every column and row, or pixel, was the intensity of the R, G or B color in



4.10 RGB image showing the resolution on X and Y axis.

that pixel ranging from 0 to 255. The resultant matrix was a 3-D matrix with dimensions which had pixel information corresponding to every color. Figure 4.10 shows a sample TLC

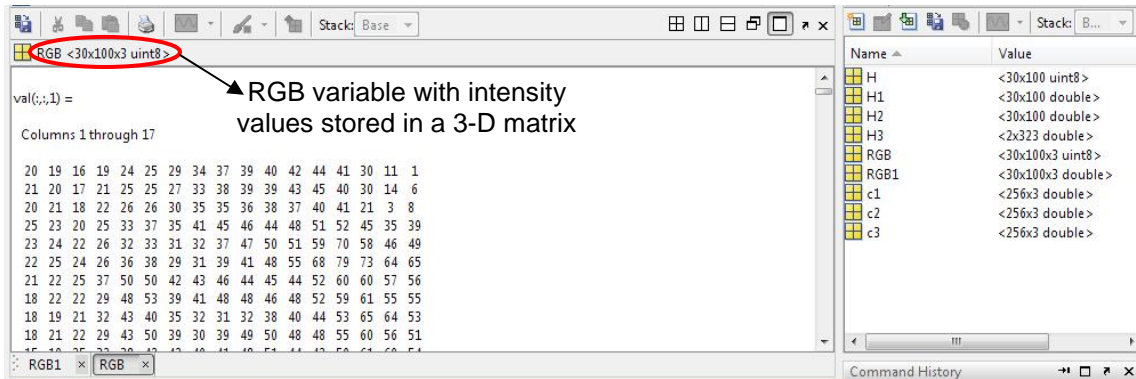


Figure 4.11 Figure showing the variable editor (left) with the pixel intensity values of RGB variable with the workspace window (right) showing the dimensions of the variables.

(Thermochromic Liquid Crystal) RGB image of 100x30 resolution which was read and stored in

the variable 'RGB'. The resultant matrix was of 30x100x3 dimensions with color intensity values displayed in every pixel in each of the 30x100 array as shown in Figure 4.11.

Referring back to figure 4.10, the darker bands in the image have lower pixel values along the respective columns of each array and the opposite for the brighter bands. The other bands have certain proportions of R, G and B to make up that color.

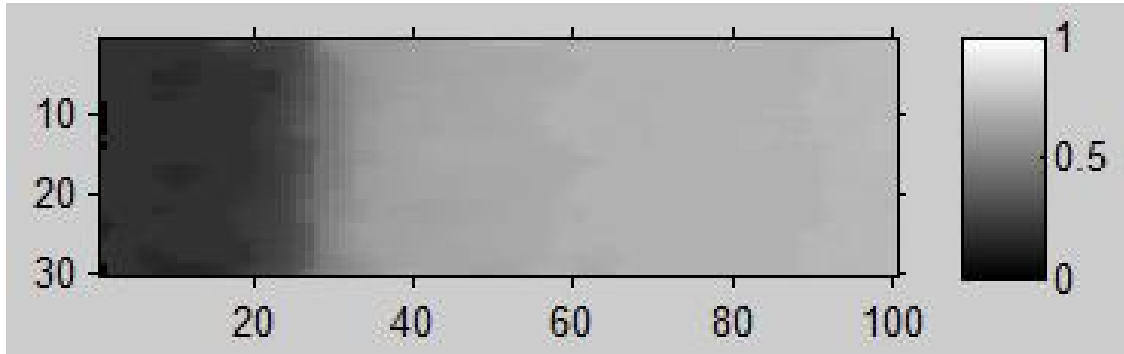


Figure 4.12 Hue image of the sample 100x30 RGB image with gray scale color bar with 256 shades.

The next step in the code (line 8) was similar to the previous step in that the hue image was read and stored in the variable 'H' which consisted of only one array of 30x100 pixels. This was due to the fact that the hue image generated in LabVIEW was an 8 bit grayscale image. Line 11 and 12 converted the RGB and H variables' pixel intensities from 0-255 (8 bit integer) range to 0-1 (double) range, as shown in Figure 4.12, in order to make the plotting of color bars more accurate. In line 14 and 16, the new variables RGB1 and H1 were plotted using the 'image' and the 'imshow' function. Image function was used to plot color images while the imshow function was used to plot the grayscale images. In line 17, c1 stored the color map for the H1 variable. A color map is a matrix containing three columns and the number of rows pertaining to the number of colors that are required to display the image. Every element in a row corresponds to intensities of red, green and blue colors ranging from 0 to 1. For example, as shown in line 17, the color map was set to a default value of 256 which meant that 256 colors were required to display the RGB or the hue image. The string 'jet' and 'gray' refers to the custom defined color or grayscale shades. Moving down to line 18, the function 'colorbar'

appended a color bar only to the hue images using 256 shades of gray. The 'caxis' command in line 18 scaled the color map axes to a minimum and maximum value. In line 20, 'flipud' command flipped the H1 hue matrix upside down, and ensured proper display of the image while plotting. This flipped the pixels on the Y axis but was not of primary concern as long as the contour regions were displayed correctly.

Until line 20 in the code, briefly summarizing the LCT process, the RGB and hue images were read into variables, their individual pixel data was converted from 8-bit integer range to double and the hue image was kept ready for the contour plotting function. The 'contourf' command in line 21 was used for this purpose. This function plotted the isolines, or

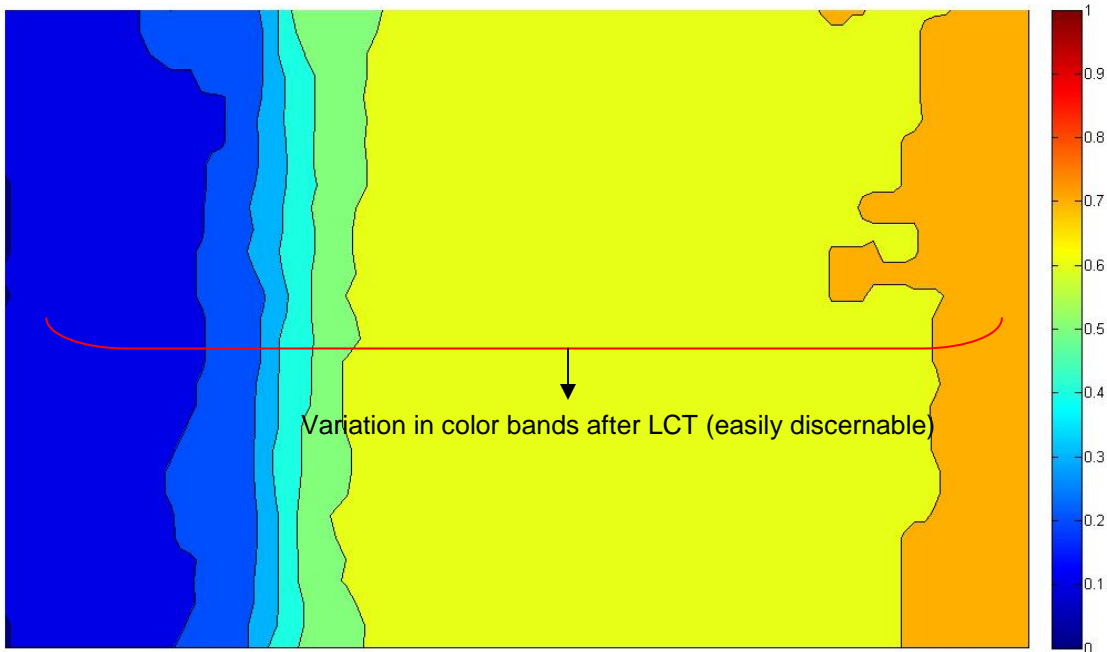


Figure 4.13 The contour plot of the hue image with the color bar purely based on the intensity values of H2.

lines within which the pixel intensities were same, in a gray scale (hue) image and filled it with a color map specified color, as shown in Figure 4.13. It was observed that by keeping the color map constant and by observing the calibration conditions of LCT as described in sub-section 4.1.1, the 'contourf' function gave the plot based on the different pixel intensities in the hue

image. Most importantly, 'contourf' returns a color plot of the hue image only and must not be mistaken with an RGB image.

Towards the end of the code, Lines 24 through 27 appended a color bar to the contour plot and labeled the temperature based on the values between ' $T_{start}^{\circ}C$ ' and ' $T_{end}^{\circ}C$ '. The next sub-section deals with the hotspot temperature to color representation in detail.

4.1.3 Temperature – Color Representation and Calibration

In order to co-relate the actual temperature values of the hotspot, as shown in Figure 4.14, to the contour plot, manual calibration of the temperature obtained at every color band of the TLC image was done. The temperature contour plot obtained in Figure 4.15(b) was based on the intensity values and the color map of the hue image as shown in Figure 4.15(a).

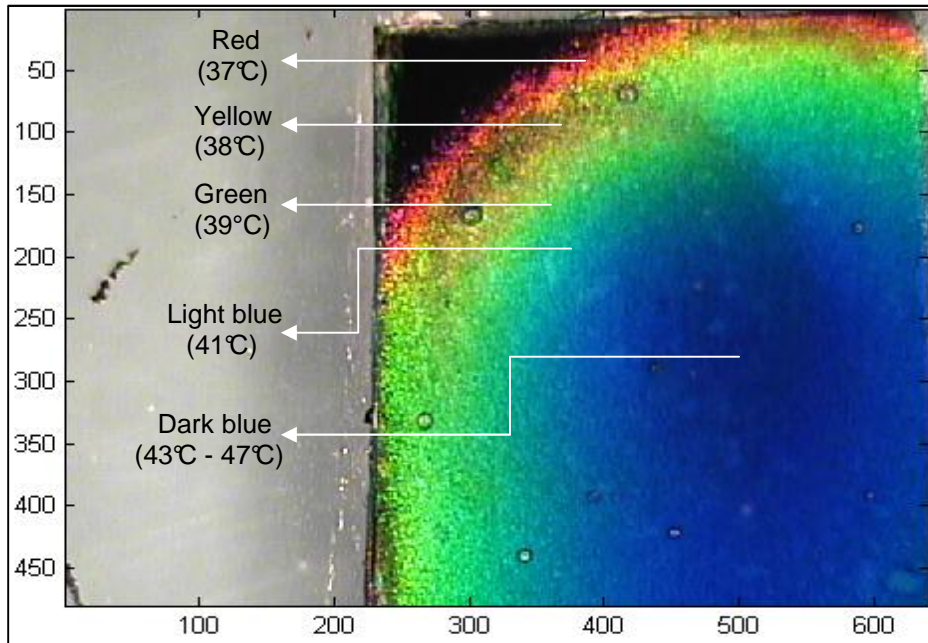
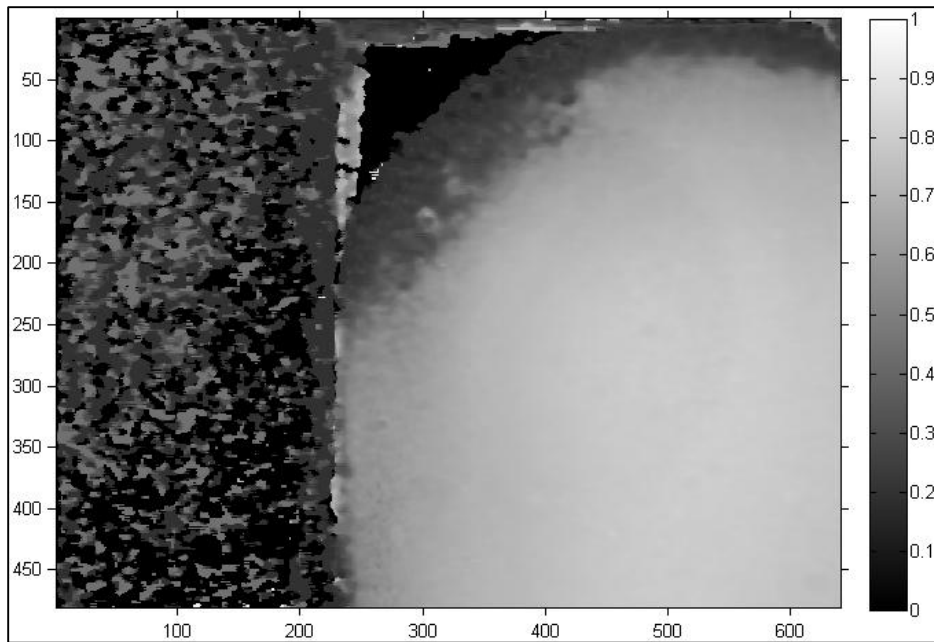
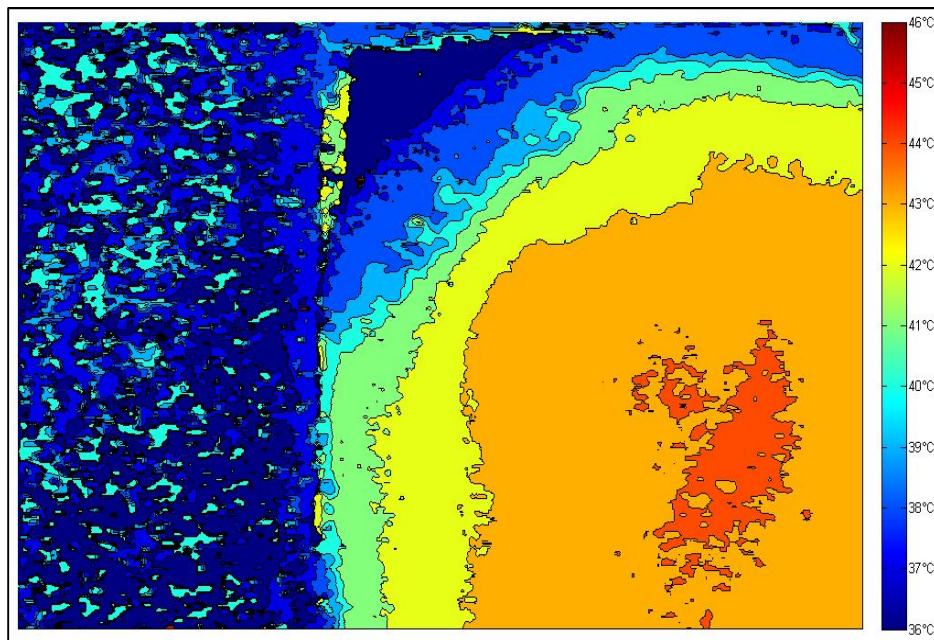


Figure 4.14 Temperature obtained at various color bands on the hot spot by using a thermocouple.

A K-type (chromel-alumel) thermocouple was used for this purpose. The calibration of the hotspot involved placing the thermocouple over the individual color band and detecting the temperature. For different runs of the experiment, the temperature values were found to be the same. Based on these values, the color bar of the contour plot was constructed.



(a)



(b)

Figure 4.15 Hue image (a) and the corresponding temperature contour (b).

The TLC used had an operating temperature range of 37°C to 45°C with a red start of 36°C and violet ending at 46°C, beyond which the LC does not show any change in color at the

center of the hotspot. Hence, the temperature range for which the color bar had to be calibrated fell within 36°C and 46°C. The remaining points on the color bar were estimated by relating the hue color map (c1) and the contour color map (c2). Hence, by referring to Figure 4.15(b), we can easily distinguish the thermal profile in the TLC image and estimate the temperature at any given point.

It has to be noted that the color bar obtained in the contour plot is not a one-to-one mapping from the original RGB image. It was obtained purely from the hue intensity values with red representing higher temperatures and blue representing lower temperatures. Most importantly, a new calibration has to be performed for a different heater and TLC setup as the hot spot temperatures change.

4.1.4 LCT Results

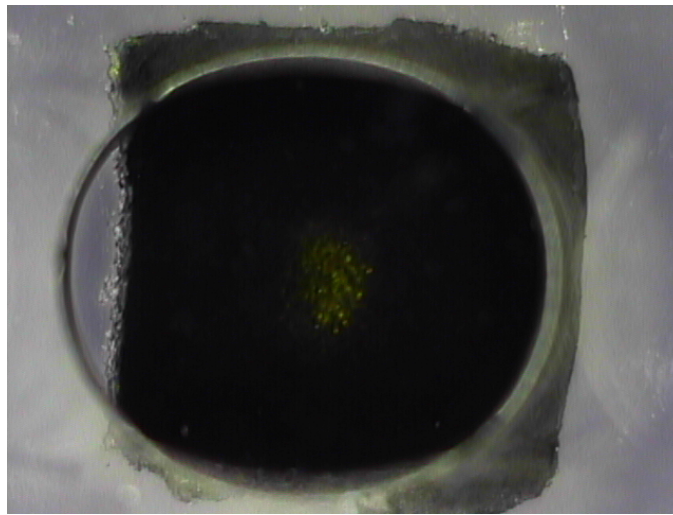
Using the LCT techniques demonstrated in the previous sub-section, different IL's were used in the device for hotspot cooling and the results were analyzed. The LC area was reduced for convenience as the device was operated at lower temperatures, while all the other device settings were kept constant.

The motive of the experiments were to use different IL's and compare it's cooling performance with that of pure de-ionized (DI) water. From LCT, the temperature change was estimated and the heat power removed by the liquid drop was calculated. This was compared to a numerically simulated result (quantitative analysis) in section 4.3.

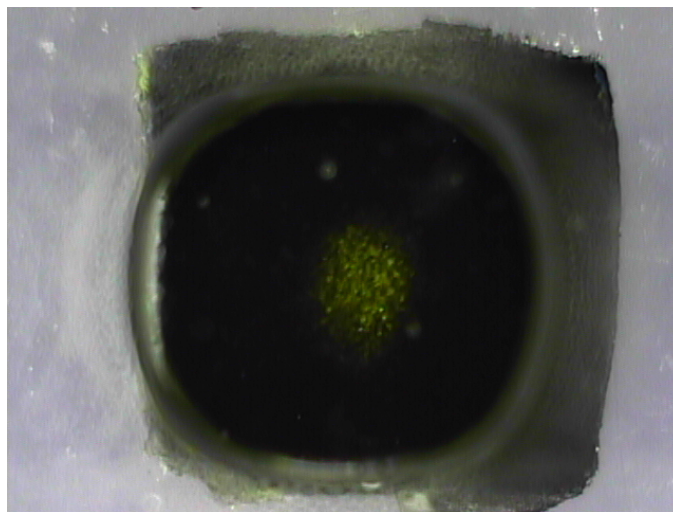
As explained in sub-section 1.3.1, three different IL's were used in the device and the results were compared to that of de-ionized (DI) water. The drops were moved over the hotspot and kept static for 5 seconds after which they were moved onto the next EWOD electrode pad.

When pure DI water was moved over the hotspot, considerable temperature change was observed on the hotspot surface. Most of this change was assumed to be dominated by the phase change phenomena of water, which can be seen clearly in Figure 4.16. It was difficult to estimate the amount of heat the DI water drop carried when it evaporated and hence the heat

carried by it was not determined. However, the change in the surface temperature of the hotspot



(a)



(b)

Figure 4.16 A DI water drop without (a) and with (b) silicone oil shell surrounded by satellite drops due to phase change effects.

was estimated by LCT and the heat power removed was estimated. An attempt was made to subdue the evaporation effects by surrounding the drop in a shell of pure silicone oil (Clearco Products Co., Inc, PA) of 1cSt viscosity, to prevent the water from evaporating. This however proved futile as phase change was still observed. The LCT results with the silicone oil core shell was worth noting as the temperature of the hotspot was found to be slightly higher than that of

pure DI water. This confirmed the fact that phase change of water drop was less severe as the silicone oil was trying to contain the water droplet within it.

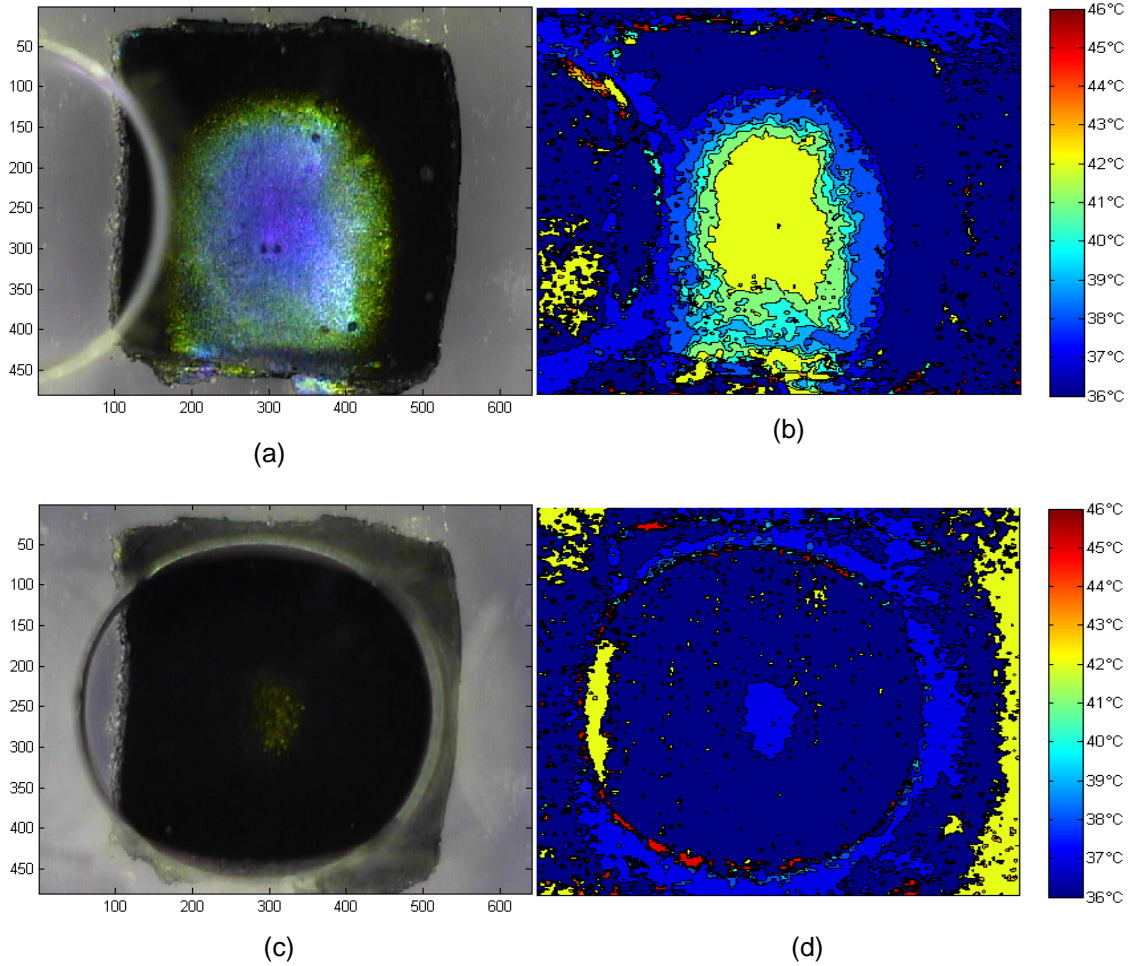


Figure 4.17 Shifted RGB and actual LCT images of pure DI water just before moving on the hotspot [(a), (b)] and after moving onto the hotspot [(c), (d)].

Figure 4.17 show the LCT results of pure DI water. Substantial phase change was observed as the drop was surrounded with satellite drops of water. It was observed that the boundary of the drop and areas around the LC paint in Fig. 4.17(d) showed signs of high temperature. This was purely due to noise and refraction effects of the light passing through the edges of the drop, and must not be mistaken for the temperature. The same holds good for all

the LCT contours. For quantitative analysis, only the contour profile within the boundary of the drop was considered.

As stated before, DI water drop with the silicone oil shell cooled the hotspot to a temperature slightly higher than that of pure DI water. The silicone oil shell did not take part in moving the drop as it is inert to EWOD. Figure 4.18 shows the results with DI water enclosed in the oil shell with the hotspot size considerably bigger than that of pure DI water.

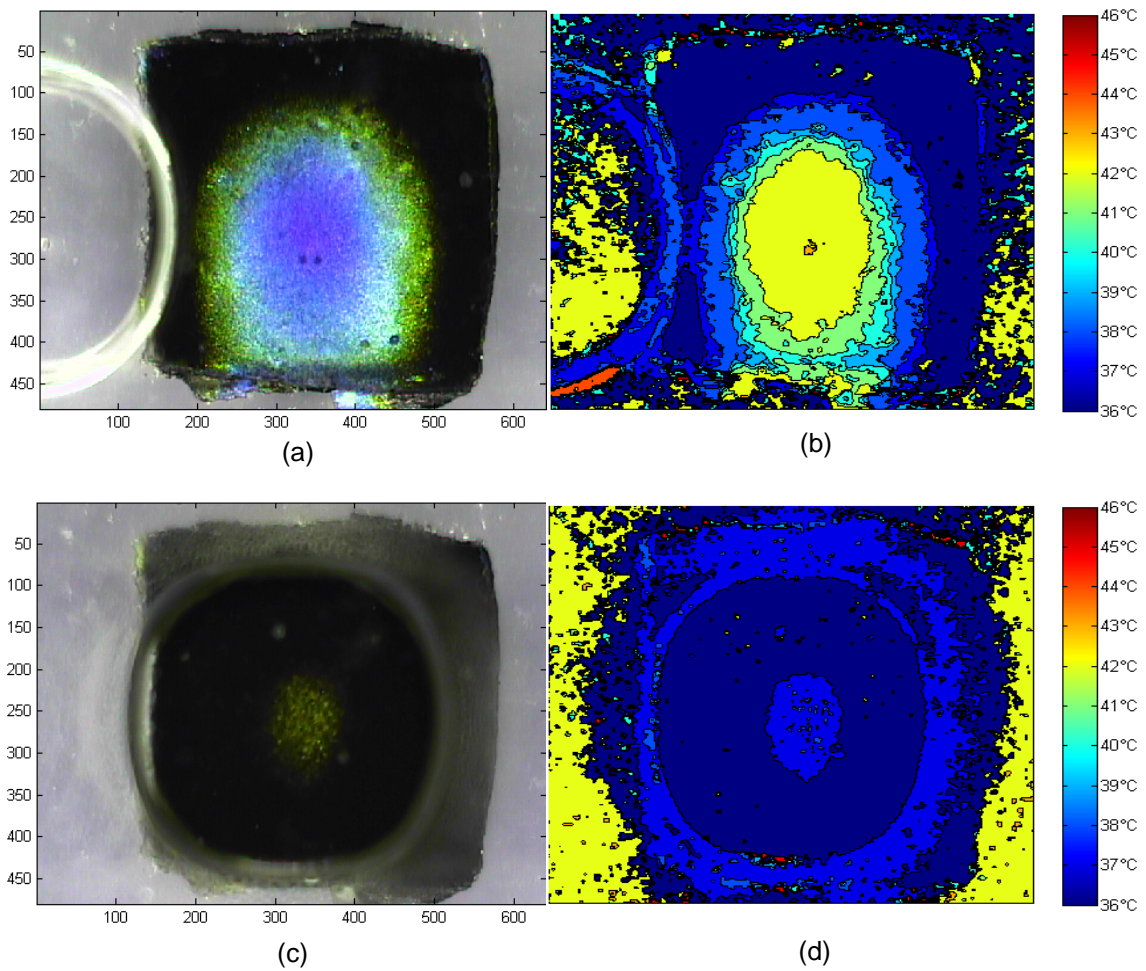


Figure 4.18 Shifted RGB and actual LCT images of pure DI water with oil shell just before cooling [(a), (b)] and after moving onto the hotspot [(c), (d)].

As with the IL's, albeit the temperature change of the hotspot was not as good as that of

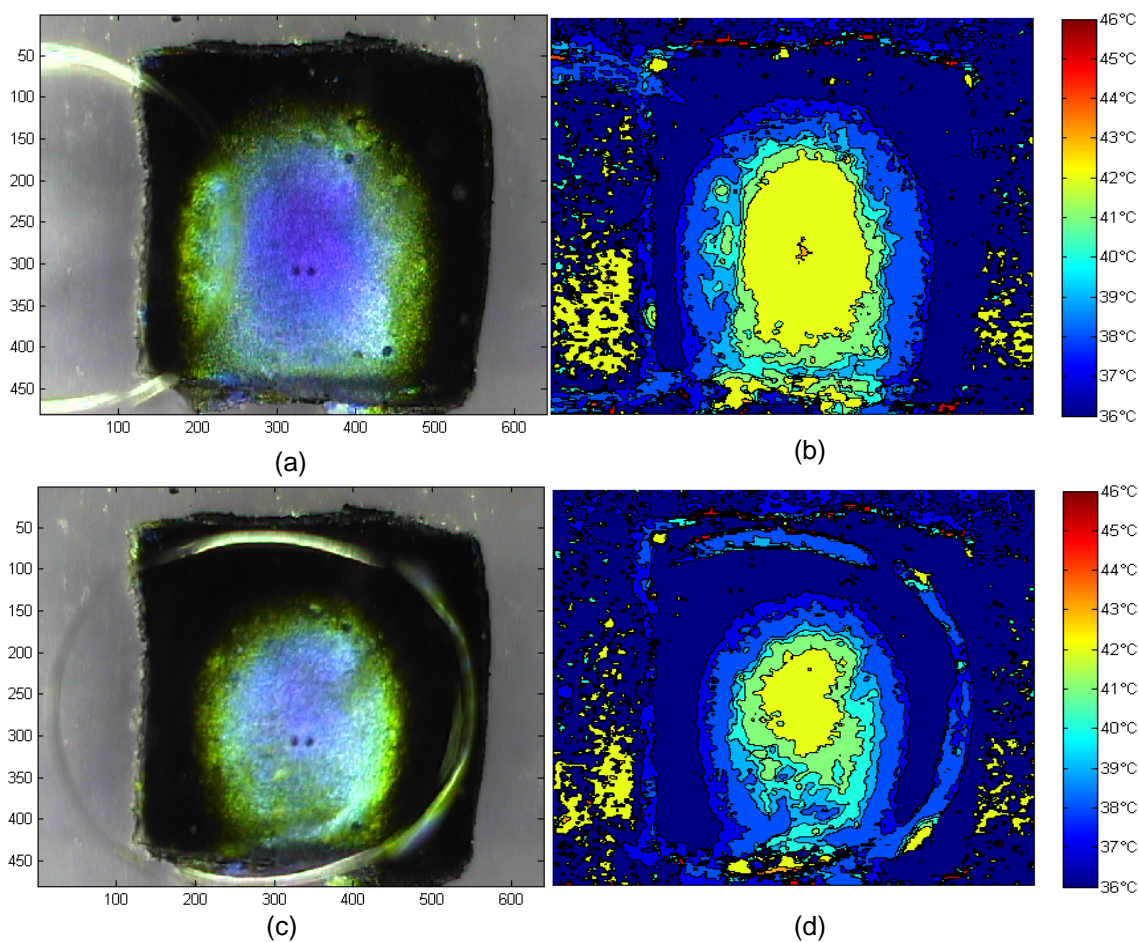


Figure 4.19 Shifted RGB and actual LCT images of IL1 just before cooling [(a), (b)] and after moving onto the hotspot [(c), (d)].

pure DI water with and without the silicone oil shell, no phase change phenomena was observed. IL1 and IL2 gave similar cooling results and IL3 gave poor cooling results. Figure 4.19 shows the cooling results with IL1 and Figure 4.20 shows the LCT results with IL2. Notice that the cooling effect was similar to IL1. The only difference that was observed during the experiment was IL1 had a larger inlet velocity than IL2 which was because IL2 had higher viscosity than IL1. Figure 4.21 shows the cooling result with IL3. IL3 was less viscous than the other ionic liquids and showed slightly better EWOD motion. The cooling results though were

worse than that of IL1 and IL2. All the experiments were performed at 150 VAC with constant heater power of 18.15 Watt.

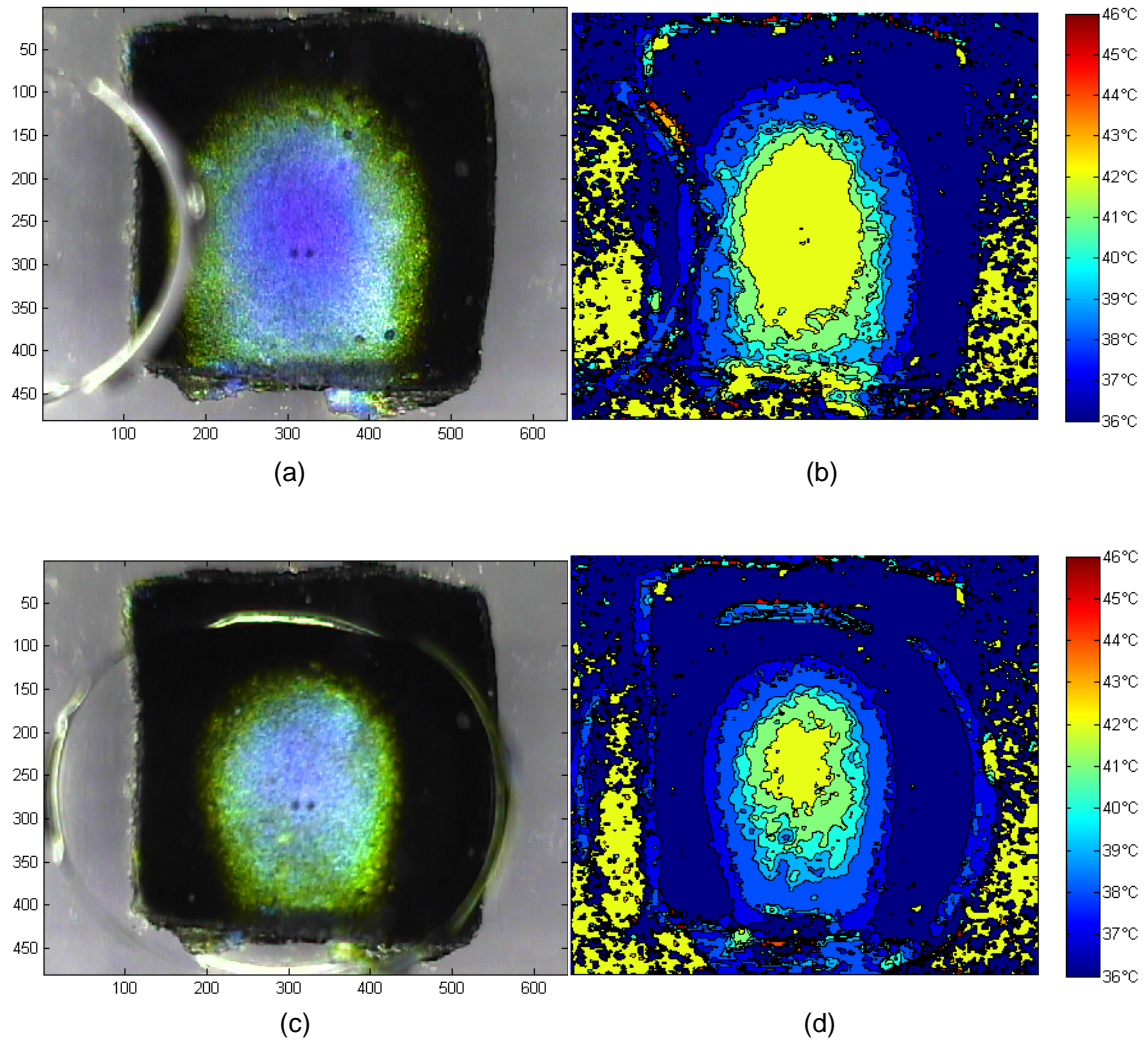


Figure 4.20 Shifted RGB and actual LCT images of pure IL2 just before cooling [(a), (b)] and after moving onto the hotspot [(c), (d)].

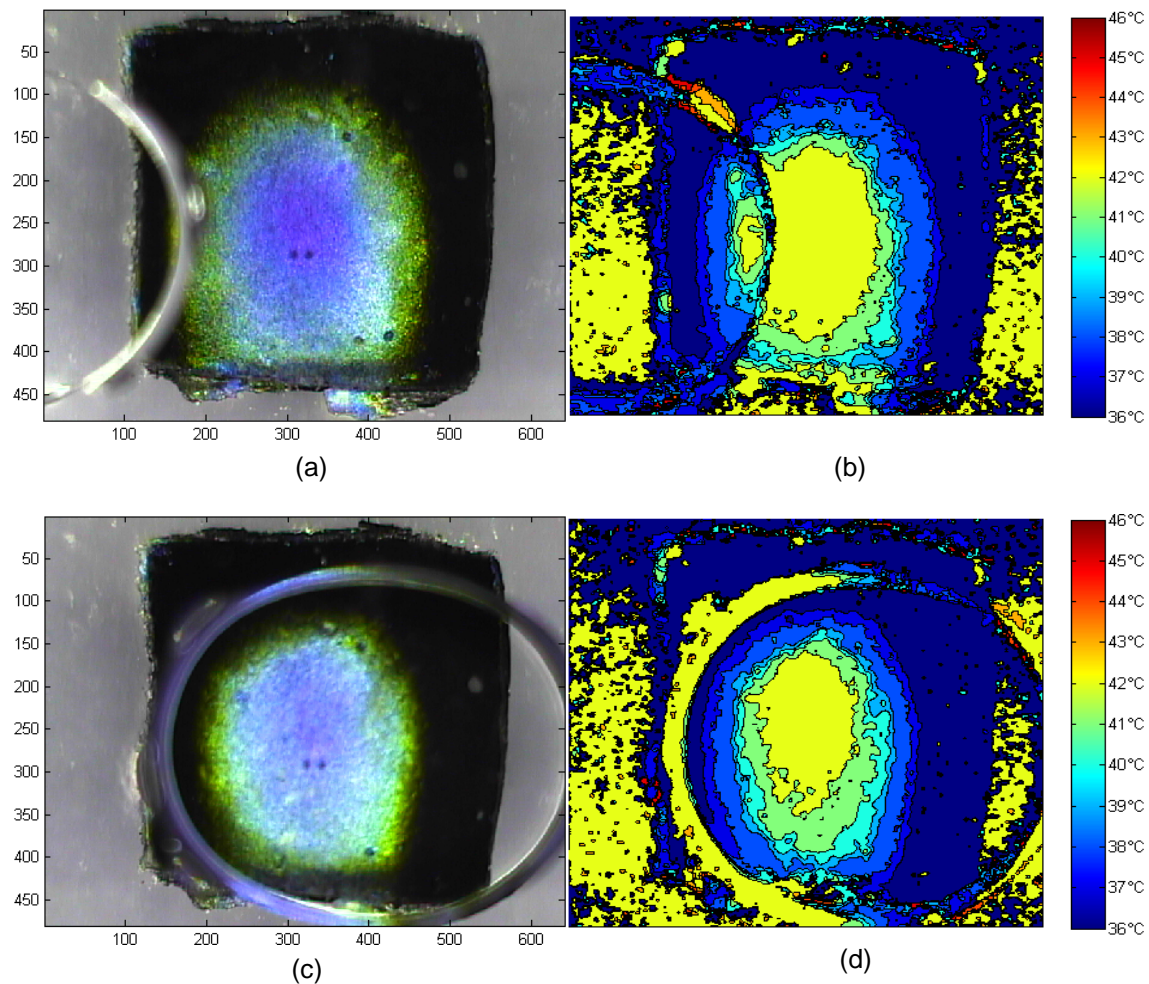


Figure 4.21 Shifted RGB and actual LCT images of IL3 just before cooling [(a), (b)] and after moving onto the hotspot [(c), (d)].

4.2 Quantitative Analysis

In this section, the LCT results obtained previously were quantified to obtain two heat transfer properties, namely, the rate of heat energy carried by the drop and the rate of heat energy transferred to the drop. The rate of heat carried by the drop depended on the average temperature change across the hotspot, which was estimated from the LCT results. In case of the heat energy transferred to the drop, only thermal conduction was considered which was calculated by estimating the area of TLC color bands at every temperature. For convenience, convection effect within the drop was not considered as it was dominated by the heat

transferred through conduction. Moreover, the convection coefficients were unknown for the IL's tested.

Both the results pointed to one conclusion – the heat removed and the heat transferred depended greatly on the heat capacity and the thermal conductivity of the liquid respectively. These results are presented in section 4.3.

4.2.1 Heat Removing Capacity

In order to calculate the rate of heat energy removed (gained) by the drop, the temperature at the liquid-solid interface (hotspot temperature) was estimated from the LCT image for 1 second of cooling time. In this time interval, the drop moved onto the hotspot from

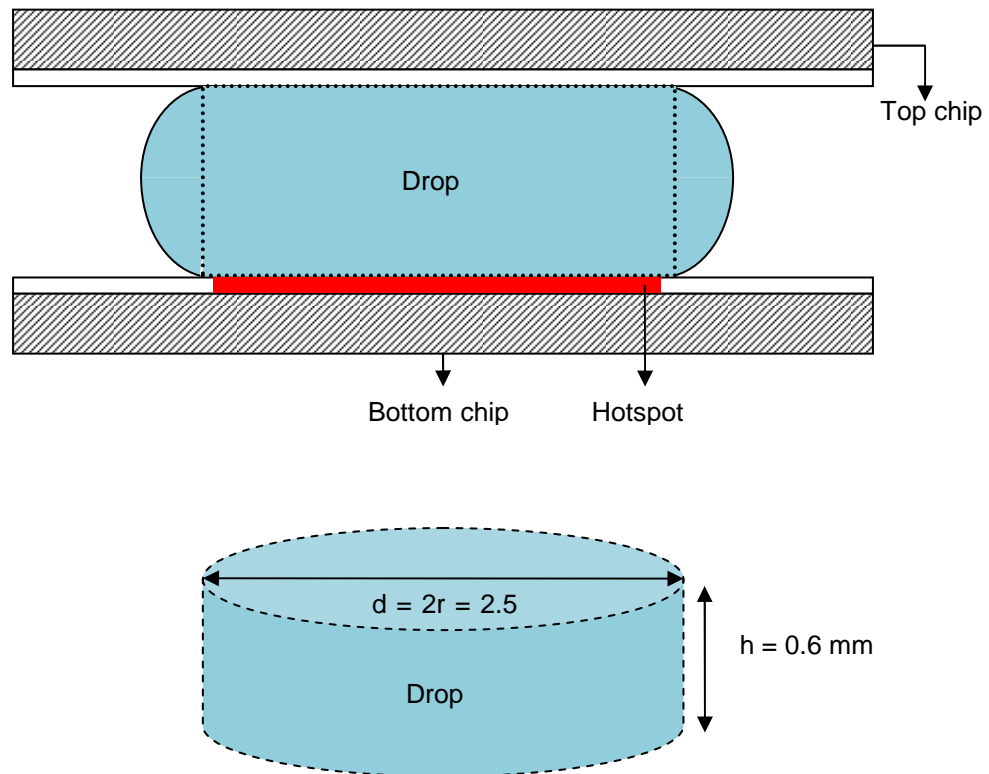


Figure 4.22 Modeling the drop as a cylinder for convenience.

the electrode pad just before the hotspot. The initial and final temperatures were considered on the same hotspot. For convenience, it was assumed that the drop took the shape of a cylinder as shown in Figure 4.22. The initial and final temperatures were calculated by considering the ratios in which the areas of the temperature bands were divided on the hotspot before and after cooling. The equation to calculate the heat energy removed is given by

$$\dot{Q} = mc(T_2 - T_1)$$

where, \dot{Q} is the heat energy rate

m is the mass of the drop

c is the specific heat capacity of the liquid

T_2 is the average hotspot temperature after cooling

T_1 is the average hotspot temperature before cooling

Volume of the drop was calculated as

$$V = \pi r^2 h = 3.14 * (1.25 \times 10^{-3} m)^2 * (0.6 \times 10^{-3} m) = 2.94e^{-9} m^3$$

The following table shows the values of \dot{Q} obtained after calculations.

Table 4.2 Table showing the heat removal rate for all the drops tested in the hotspot cooling device

Liquid	Density of liquid $\rho (Kg * m^{-3})$	Mass of liquid drop m $= \rho \times V (Kg)$	Heat capacity $c (J * Kg^{-1} * K^{-1})$	$T_1 (K)$	$T_2 (K)$	Approximate $\dot{Q} (W)$
DI water	1000	$2.94e^{-6}$	4220	311.34	309.09	0.027
IL1	1100	$3.23e^{-6}$	1571	311.7	311.36	0.0012
IL2	1290	$3.79e^{-6}$	1350	311.79	311.4	0.0019
IL3	1430	$4.20e^{-6}$	1727	312.03	311.53	0.003

4.2.2 Heat Transferred through Conduction

The drop over the hotspot was idealized as a solid disc with thermal conductivity ' k '. The thermal conductivities of all the liquids were calculated with the help of a custom built²⁷ thermal conductivity measurement meter. The rate of heat energy transferred through conduction was estimated by calculating the area of every color band in the LCT image. This was done using NI Vision Assistant 9.0 software.

In Vision Assistant, the LCT image was processed and a histogram estimation of the image was performed. This function counted the total number of pixels in each color band and generated an excel sheet. Figure 4.23 shows this process. In order to get accurate estimation of

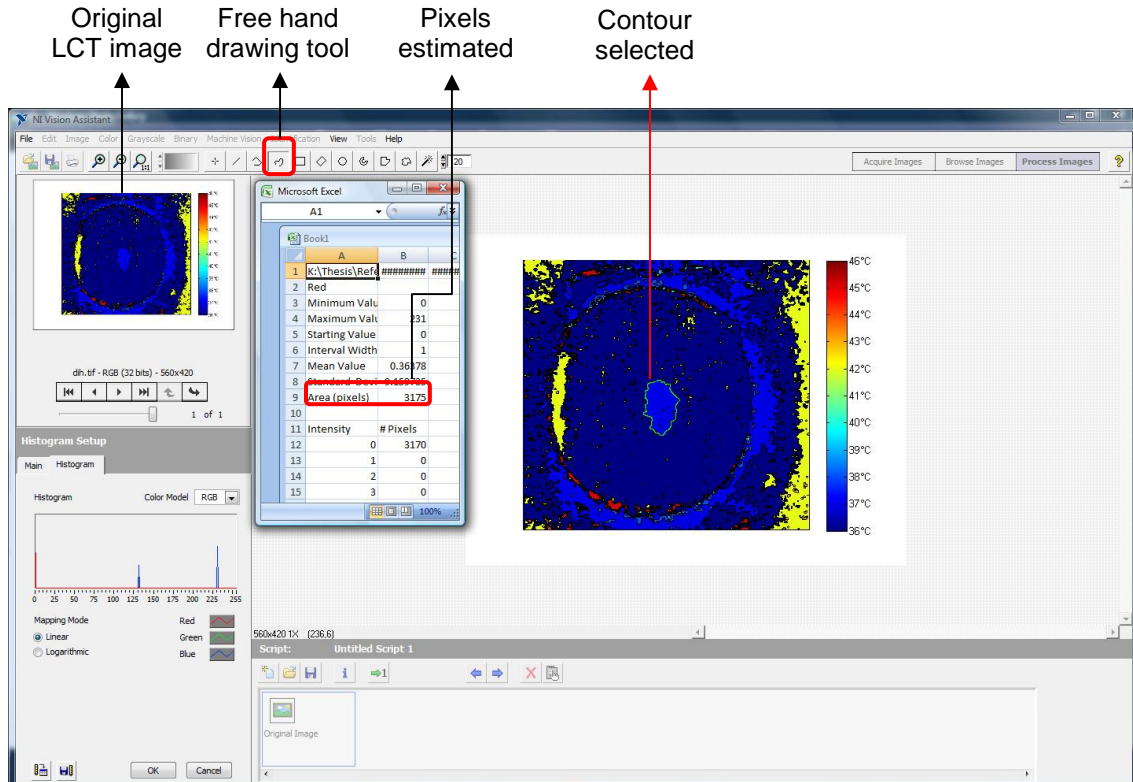


Figure 4.23 Figure showing the pixels estimation in each color band on the LCT image.

the pixels in the color band, the free hand drawing tool was used to select the correct contour so that the histogram function could calculate the pixels within the contour drawn. In order to estimate the area of the pixels in a given color band, the area of one pixel was estimated. This

was calculated by dividing the length of each side of the LCT image, which was same for all images, by the number of pixels along that side. The length of the side of the image was considered when the image was displayed on the screen at normal zoom.

In figure 4.24, the lengths of the sides were calculated as 97 mm and 103 mm respectively. Each of these dimensions was divided by the total number of pixel rows and pixel columns to get the dimension of each pixel.

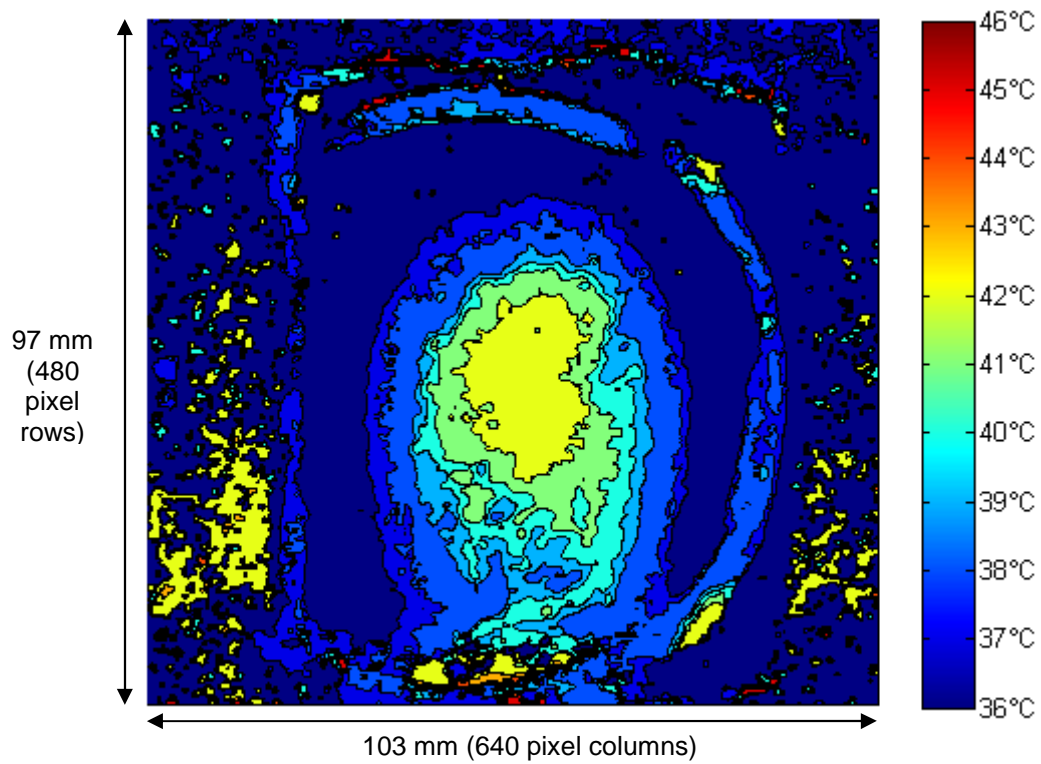


Figure 4.24 Actual dimensions of the LCT image displayed at normal zoom.

The dimensions of the pixels are

$$y - \text{dimension of each pixel} = 0.20 \text{ mm}$$

$$x - \text{dimension of each pixel} = 0.16 \text{ mm}$$

$$\text{Area of each pixel} = 0.2 * 0.16 = 0.032 \text{ mm}^2$$

Once the area of the pixel was known, this value was multiplied with the number of pixels in

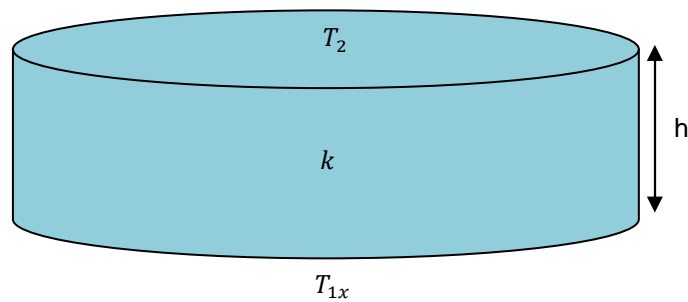
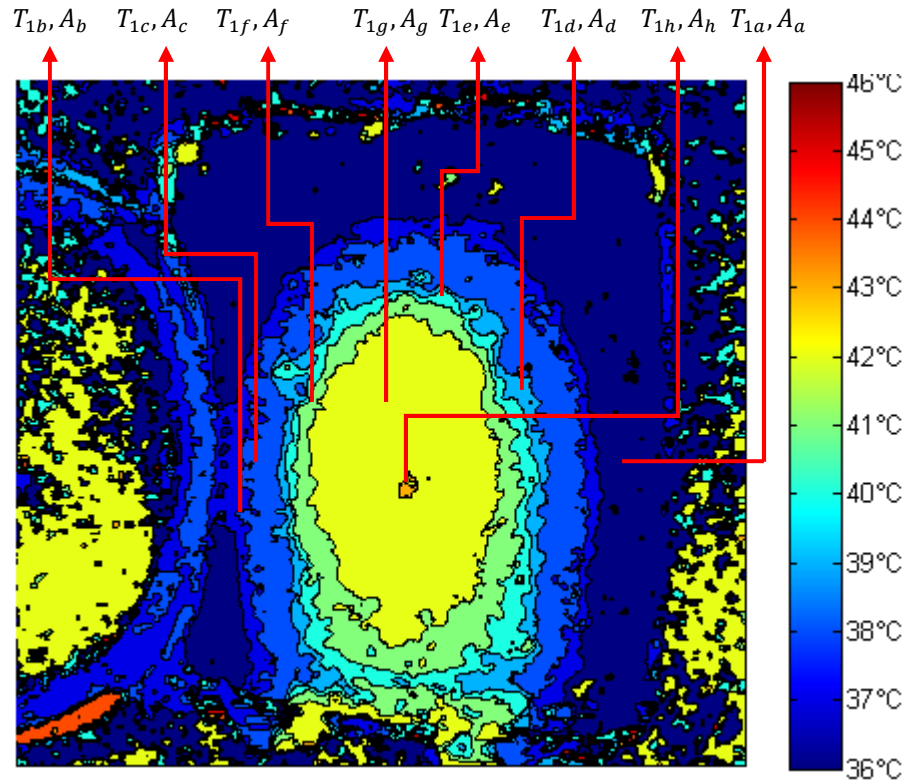


Figure 4.25 Figure showing the temperature and area of each color band on the hotspot (2-D) and the temperature distribution in the drop (3-D). The x in T_{1x} takes variables from a to h.

each color band to get the area of the color band. The areas and the temperatures of the individual bands were estimated as shown in Figure 4.25. As shown in Figure 4.25, the drop was assumed to be a cylindrical disk of constant thermal conductivity, 'k', and top side temperature, T_2 , applying Fourier's Law of heat conduction, the net rate of heat transferred, \dot{Q}_{net} , is given by

$$\dot{Q}_{net} = \dot{Q}_a + \dot{Q}_b + \dot{Q}_c + \dot{Q}_d + \dot{Q}_e + \dot{Q}_f + \dot{Q}_g + \dot{Q}_h$$

or

$$\begin{aligned} \dot{Q}_{net} = k * A_a * \frac{T_2 - T_{1a}}{h} + k * A_b * \frac{T_2 - T_{1b}}{h} + k * A_c * \frac{T_2 - T_{1c}}{h} + k * A_d * \frac{T_2 - T_{1d}}{h} + k * A_e \\ * \frac{T_2 - T_{1e}}{h} + k * A_f * \frac{T_2 - T_{1f}}{h} + k * A_g * \frac{T_2 - T_{1g}}{h} + k * A_h * \frac{T_2 - T_{1h}}{h} \end{aligned}$$

In the above equation, the A values were calculated by estimating the number of pixels in each color band as explained before and multiplying it by the area of each pixel as calculated.

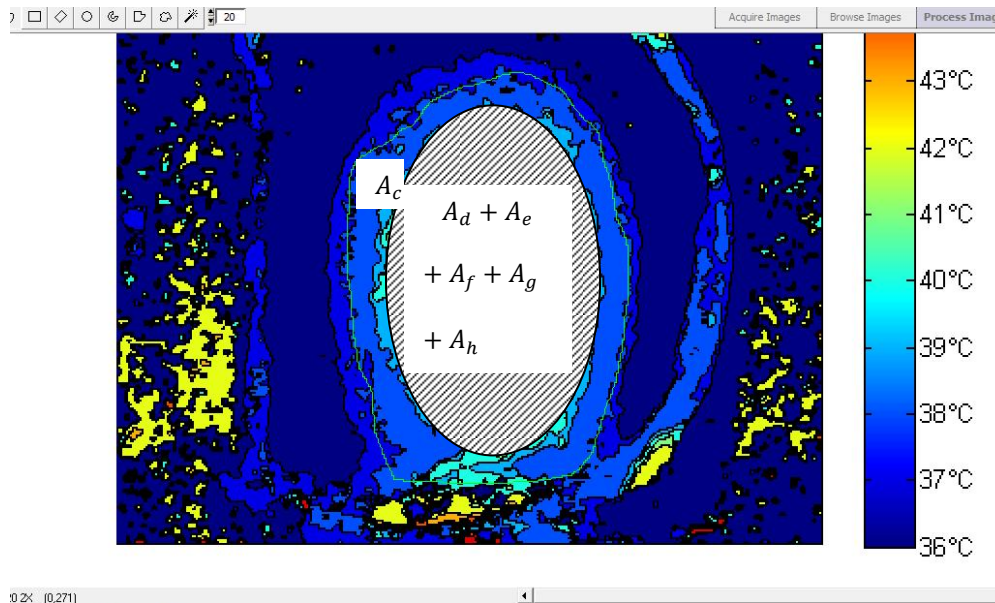


Figure 4.26 Estimation of A_c by subtracting A_d , A_e , A_f , A_g and A_h .

In case of IL's where we see more than one color bands, the areas for every color band was calculated and was subtracted from the area of the band surrounding it as shown in Figure 4.26.

Table 4.3 Table showing the net heat transferred through conduction

Color band	Area of color band A_x (m^2)				T_{1x} (K)	T_2 (K)	k ($W * m^{-1} * K^{-1}$)				\dot{Q}_x (W) transferred to drop					
	DI wate	IL1	IL2	IL3			DI	IL1	IL2	IL3	DI wate	IL1	IL2	IL3		
Band a	17.5 x 10^{-7}	7.6 x 10^{-7}	10.8 x 10^{-7}	8.25 x 10^{-7}	309	298							17.9 x 10^{-3}	2.64 x 10^{-3}	3.36 x 10^{-3}	2.57 x 10^{-3}
Band b	0.82 x 10^{-7}	2.16 x 10^{-7}	3.6 x 10^{-7}	2.83 x 10^{-7}	310	298							0.91 x 10^{-3}	0.82 x 10^{-3}	1.22 x 10^{-3}	0.96 x 10^{-3}
Band c	-	3.35 x 10^{-7}	5.2 x 10^{-7}	3.24 x 10^{-7}	311.2	298							0	1.40 x 10^{-3}	1.94 x 10^{-3}	1.21 x 10^{-3}
Band d	-	1.08 x 10^{-7}	2.88 x 10^{-7}	1.44 x 10^{-7}	312	298							0	0.47 x 10^{-3}	1.14 x 10^{-3}	0.57 x 10^{-3}
Band e	-	0.36 x 10^{-7}	1.44 x 10^{-7}	1.08 x 10^{-7}	313	298	0.56	0.19	0.17	0.17			0	0.17 x 10^{-3}	0.612 x 10^{-3}	0.45 x 10^{-3}
Band f	-	3.34 x 10^{-7}	0.72 x 10^{-7}	2.88 x 10^{-7}	314	298							0	1.69 x 10^{-3}	0.32 x 10^{-3}	1.30 x 10^{-3}
Band g	-	2.19 x 10^{-7}	2.16 x 10^{-7}	3.60 x 10^{-7}	315.2	298							0	1.19 x 10^{-3}	1.05 x 10^{-3}	1.75 x 10^{-3}
Band h	-	-	-	-	316.5	298							0	0	0	0
\dot{Q}_{net} transferred to the drop																
													18.81 x 10^{-3}	8.38 x 10^{-3}	9.64 x 10^{-3}	8.81 x 10^{-3}

Moreover, while calculating the actual area of the color band on the TLC, a scaling factor was considered. The factor of 888 was calculated by taking the ratios of the actual dimensions on the hotspot and the image dimensions as displayed on the screen.

Following all the steps as mentioned above, the net heat transfer rate \dot{Q}_{net} for each liquid was calculated and published in Table 4.2 in the previous page.

4.2.3 Results

In sub-sections 4.2.1 and 4.2.2, the rate of heat removed and the heat transferred to the drop were calculated. It was observed that DI water had a maximum heat removal rate of 0.027 Watt and IL1 had the lowest rate of 0.0012 Watt. Among the IL's IL3 had the maximum heat removal rate of 0.003 W. The rate of heat transferred through conduction was highest for DI water and lowest for IL1. DI water, among all liquid's, had a highest rate of $18.81 \times 10^{-3} W$. Among all IL's, IL2 gave a maximum conduction rate of $9.64 \times 10^{-3} W$ while IL1 gave the lowest rate of $8.38 \times 10^{-3} W$.

4.3 Conclusions and Future Work

In the previous section, the values of the rate of heat removed and heat transferred was calculated with the help of LCT. It was observed that the heat removal and the heat transfer rate for DI water were highest for unit time interval. This was due to the fact that DI water had a higher heat capacity and thermal conductivity values. IL's had a lower heat removal and heat transfer rates attributed to lower heat capacity and conductivity values. Among the IL's, IL3 had the highest heat removal rate while IL1 had the lowest. The heat conduction rate was highest for IL2 and lowest for IL1 transfer rate. It has to be noted that the heat removal rate was a rough approximation as the values of the dark blue band surrounding the hotspot before cooling were taken as a uniform temperature value. This was due to the fact that the operating range of the TLC paint fell in the range of 36°C to 46°C.

From the above conclusions, it was observed that the qualitative and the quantitative results conformed well to the basic heat transfer laws, with DI water emerging as the best liquid

for heat transfer. Albeit IL's have special properties which are better than water based coolants, it was disappointing to learn that they performed poorly in cooling the hotspot. There are ways to enhance the cooling ability and efforts are being made to increase the thermal conductivities of IL's by adding CNT's. Due to the fact that use of CNT's in the device for hotspot cooling made it difficult to observe the TLC image, it was not analyzed.

In general, the low conduction rates showed that the heat lost through the surroundings was high. This calls for better insulating and packaging methods. In the near future, with the use of high conductivity ionic liquids, combined with better ways of analyzing temperature changes on the hotspot, and by improving the device design, the potential of IL's for electronic hotspot cooling can be explored to greater depths with promising results.

APPENDIX A
MATLAB CODE FOR LCT

The following code describes the LCT operations in detail using MATLAB's Image

Processing Toolbox.

```
1  % Code to image read, reading hue intensity values, filter out noise,
2  % relate hue values to true color and plot colorbar, plot color image % from colorbar,
3  % add temp. % colorbar to color image, plot graph between % hue and temperature...
4  % © Shreyas Govindraj
5  clc;close all;clear all;
6  %% Image read - RGB and Hue
7  RGB=imread('RGB.bmp');
8  H=imread('Hue.bmp');
9  %% Converting 8 bit unsigned integers to double precision floating point
10 % for greater accuracy
11 RGB1=double(RGB)/255;
12 H1=double(H)/255;
13 %% Plot RGB1 & H1
14 image(RGB1);
15 figure; % Open new figure window
16 imshow(H1);axis on;
17 c1=colormap(gray(256)); % color intensity values of Hue (256 shades of gray)
18 colorbar;caxis([0 1])
19 %% Converting hue to color
20 H2=flipud(H1);
21 figure;H3=contourf(H2);
22 c2=colormap(jet(256)); % color intensity of standard colormap
23 colorbar;caxis([0 1]);axis off;
24 %% Label colorbars with temperature
```

```
25  cb=colorbar('YTickLabel',{T_start°C','T_1°C','T_2°C','T_3°C',...
26  T_end-1°C','T_end°C'});
27  set(cb,'XTickMode','manual');
```

REFERENCES

- [1] S. Lee, "Optimum design and selection of heat sinks", Eleventh IEEE SEMI-THERM Symposium, 1995, pp. 48-54.
- [2] M. Groll et al., "Thermal control of electronic equipment by heat pipes", *Rev. Gen. Therm.*, Elsevier, 1998, Vol. 37, pp. 323-352.
- [3] D. S. Kercher et al., "Micro jet cooling devices for thermal management of electronics", *IEEE Transactions on Components and Packaging Technologies*, June 2003, Vol. 26, No. 2, pp. 359-366.
- [4] S. H. Moon and G. Hwang, "Development of the micro capillary pumped loop for electronic cooling", *THERMINIC 2007*, September 2007, ISBN: 978-2-35500-002-7.
- [5] E. G. Colgan et al., "A practical implementation of silicon microchannel coolers for high power chips", *IEEE Transactions on Components and Packaging Technologies*, June 2007, Vol. 30, No. 2, pp. 218-225.
- [6] H. Moon et al., "Low voltage electrowetting-on-dielectric", *Journal of Applied Physics*, October 2002, Vol. 92, No. 7, pp. 4080-4087.
- [7] F. Mugele et al., "Electrowetting: from basics to applications", *Journal of Physics: Condensed Matter*, 2005, pp. 705-742.
- [8] C. Quilliet and B. Berge, "Electrowetting: a recent outbreak", *Current Opinion in Colloid and Interface Science*, Elsevier, 2001, Vol. 6, pp. 34-39.
- [9] J. Lee et al., "Electrowetting and electrowetting-on-dielectric for microscale liquid handling", *Sensors and Actuators A 95*, Elsevier, 2002, pp. 259-268.
- [10] B. Berge, "Electrocapillarity and wetting of insulator films by water", *Comptes Rendus de l'Academie des Sciences Serie II*, 1993.
- [11] P. Paik et al., "Droplet-based hotspot cooling using topless digital microfluidics on a printed circuit board", *THERMINIC 2005*, EDA Publishing Association, 2007.
- [12] V. Pamula et al., "Cooling of integrated circuits using droplet-based microfluidics", *Great Lakes Symposium on VLSI, Proceedings of the 13th ACM Great Lakes symposium on VLSI*, 2003, pp. 84-87.
- [13] H. Oprins et al., "Selective cooling of microelectronics using electrostatic actuated liquid droplets – modeling and experiments", *THERMINIC 2004*, Laboratoire TIMA, pp. 207-212.
- [14] E. Baird and K. Mohseni, "Digitized heat transfer: a new paradigm for thermal management of compact micro systems", *IEEE Transactions on Components and Packaging Technologies*, March 2008, Vol. 31, No. 1, pp. 143-151.

- [15] S. Millefiorini et al., "Electrowetting of ionic liquids", *J. Am. Chem. Soc.*, 2006, Vol. 128, pp. 3098-3101.
- [16] L. C. Branco et al., "Preparation and characterization of new room temperature ionic liquids", *Chem. Eur. J.*, 2002, Vol. 8, No. 16, pp. 3671-3677.
- [17] Y. Nanayakkara et al., "A fundamental study on electrowetting by traditional and multifunctional ionic liquids: possible use in EWOD microfluidic applications", *Anal. Chem.*, 2008, Vol. 80, pp. 7690-7698.
- [18] Y. Nanayakkara et al., "The role of AC frequency on electrowetting of traditional and multifunctional ionic liquids", submitted to *Anal. Chem.*, 2009.
- [19] A. Kumar et al., "Finite conductivity effects and apparent contact angle saturation in AC electrowetting", *Dynamics in small confining systems*, 2005, Vol. 899E, 0899-N06-01.1 to 0899-N06-01.8.
- [20] J. Zhang et al., "Polymerization optimization of SU-8 photoresist and its applications in microfluidic systems and MEMS", *Journal of Micromechanics and Microengineering*, 2001, Vol. 11, pp. 20-26.
- [21] "TLC products for use and testing in research applications", LCR Hallcrest Research and Testing Products,
<http://www.hallcrest.com/downloads/RT001%20R&T%20Prods%20Info%20Package.pdf>
- [22] V. U. Kakade et al., "Accurate heat transfer measurements using thermochromic liquid crystal. Part 1: Calibration and characteristics of crystals", *International Journal of Heat and Fluid Flow*, Elsevier, 2009, pp. 1-11.
- [23] R. Muwanga and I. Hassan, "Local heat transfer measurements in microchannels using liquid crystal thermography: Methodology, development and validation", *Journal of Heat Transfer*, 2006, Vol. 128, pp. 617-626.
- [24] D. R. Sabatino et al., "A high-accuracy calibration technique for thermochromic liquid crystal temperature measurements", *Experiments in Fluids*, Springer-Verlag, 2000, Vol. 28, pp. 497-505.
- [25] http://upload.wikimedia.org/wikipedia/commons/b/b6/HSL_HSV_cylinder_color_solid_comparison.png
- [26] MATLAB help.
- [27] Courtesy: Jagath Nikapitiya, UTA.

BIOGRAPHICAL INFORMATION

Govindraj Shreyas Bindignavale received his Bachelor of Engineering degree in Mechanical Engineering from Osmania University, India, in May 2007. He is currently pursuing his Master of Sciences degree in Mechanical Engineering at The University of Texas at Arlington, USA. He is a member of the Integrated Micro & Nanofluidic Systems Lab, guided by Hyejin Moon. His research interests include heat transfer, microfluidics and MEMS device fabrication with emphasis on Computer-aided design (CAD) and engineering (CAE).